GEOPHYSICAL INVESTIGATION OF FAULTS AND FRACTURES IN KIAMUNYI AREA SOUTH WEST OF MENENGAI VOLCANO IN THE KENYA RIFT

NJERU RITA MWENDIA

A Thesis Submitted to the Graduate School in Partial Fulfilment for the Requirements of the Award of Master of Science Degree in Physics of Egerton University

EGERTON UNIVERSITY

JUNE, 2016

DECLARATION AND RECOMMENDATION

DECLARATION

This thesis is my original work and has not been submitted in part or whole for an award in any institution.

NJERU RITA MWENDIA

SM13/3362/12

Signature……..... Date…….....

RECOMMENDATION

This thesis has been submitted with our approval as supervisors for examination according to Egerton University regulations.

Dr. A. M. WAMALWA

Geothermal Development Company

Signature…… Date……..

Dr. M.S.K KIRUI

Egerton University

Signature……..... Date…….

COPY RIGHT

ACKNOWLEDGEMENT

I owe a sincere debt of gratitude to the Almighty God whose grace is always abounding for the care and protection He gave me throughout the research period.

I acknowledge my tireless supervisors, Dr. A. M. Wamalwa and Dr. M.S.K. Kirui for their advice, sincere guidance, for providing me the opportunity to do this work and their precious questions and insights throughout my research which have allowed me to see this research through. I am blessed to have had mentors with such a Christ-like attitude. A hearty thank you is also owed to Mr. Majanga for his helpful insights and suggestions.

A lot of thanks also go to the Kenya Energy generating Company (KENGEN) for giving me a chance to train with their Geophysics team. In particular I thank the Senior Geophysicist-2014, Madam Ann, for organizing my training timetable and Mr. Charles Ogada who saw me through the data collection exercise as well as the entire KENGEN Geophysics team. I acknowledge the assistance offered by the Kiamunyi area administration that ensured a safe working condition through the help of the area sub chief. I also thank all the field assistants who were always there for me during the data collection exercise.

I acknowledge the Egerton University Graduate School for funding my research project in 2013/2014 financial year. I greatly appreciate the members of staff in the Faculty of science Dean's office and in the Physics Department particular for creating a conducive and enabling environment for my research work to be accomplished. It is quite evident that they truly care about the welfare of the students that they serve so well. I would also like to thank my graduate student colleagues; Mrs. Hellen Owiti and Mr. Kallen Mulilo for their moral support, advice and encouragement during this research period.

I also wish to thank the Nakuru county government for permitting me to do this research. Special thanks to all the residents in the study region who allowed me to trespass their precious homesteads and farms during the data collection exercise. This showed great support to this specific research and my education as well.

Finally, I thank my dear mum Mrs. Juliet Njeru and the entire Njeru's family for all the encouragement and financial support to see this work through. It's through their tireless prayers that this research was completed. May God bless you all.

DEDICATION

I dedicate this work to the entire Njeru's family. All of whom I attribute my success to their unconditional support. In particular, I dedicate this work to my mum Mrs. Juliet Njeru and my Nephew Dennis Mugambi.

ABSTRACT

The rapidly growing Nakuru town needs expansion to accommodate the increasing population. This vast expansion can only be done at the outskirts of the town. However, no single research has been done with the aim of checking the geological stability of the regions around Nakuru town; either by mapping new fault zones or by confirming using geophysical methods the presence of faults shown on geological maps. Kiamunyi estate being in the outskirts of the town was therefore chosen for this research; to evaluate the stability of the area for development. The resistivity and potential methods were employed in this study. Five apparent resistivity curves were plotted on a log-log graph using the sounding data. From the curves, the study area was found to have three layers to the basement rock. Using the horizontal electrical resistivity data, a resistivity contour map was generated. Two resistivity profiles were also plotted. From these, a low resistivity region that was sandwiched between two highly resistive regions was observed. Gravity and magnetic data were contoured and interpreted. From the gravity contour map, a gravity low was observed between two gravity highs. A low magnetic intensity zone that occurred between two high magnetic intensity regions was also evident. An interpretation was made that the low resistivity region observed between high resistivity regions, low gravity region observed between high gravity regions and low magnetic intensity region observed between high magnetic intensity regions observed on the western side indicate the presence of fractured rocks. These anomalies are observed at the same region where there is a trench like depression on the surface about 30 m wide. The location of these anomalies from the resistivity, gravity and magnetic contour maps coincides. It is therefore concluded that the observed anomalies indicate the presence of a fault zone that strikes Northwest-Southeast. Construction around the faulted zone should be carefully planned and where possible reinforcement done. More research can also be done to map other faults cutting across the whole of Kiamunyi estate and its surrounding. Seismic stations can also be set to monitor the activity of the fault zones. If the faults are observed to be active then construction around the zones should be discouraged. To curb the water scarcity in Kiamunyi, ground water exploration can be done along the mapped fault zone since faults form paths for underground water flow.

TABLE OF CONTENTS

LIST OF FIGURES

LIST OF ABBREVIATIONS AND ACRONYMS

dc	Direct current
GPS	Global Positioning System
HEP	Horizontal Electrical Profiling
Ka	Thousand years
mGal	Miligals
SAS	Signal Averaging System
VES	Vertical Electrical Sounding

CHAPTER ONE

INTRODUCTION

1.1 Background information

Kiamunyi area is located within the Kenya Rift Valley which lies within the East African Rift Valley. Kiamunyi is one of the estates of Nakuru town to the west at the foot of the Menengai volcano to the south west. Several geophysical studies have been done around the Menengai volcano focusing on geothermal exploration (Simiyu and Keller, 2001; Mariita and Keller, 2007; Simiyu, 2009; Wamalwa *et al*., 2013). The main focus has however been in the Menengai volcano, though case studies have also focused on Nakuru town (Ngecu and Nyambok, 2000). Studies have shown that Nakuru town has experienced subsidence in the past leading to damage of property in addition to landscape and environmental degradation (Ngecu and Nyambok, 2000). Their study suggested that the underlying cause of these subsidences could be buried faults covered by volcanic deposits. These subsidences are mainly collapse of unconsolidated sediments occurring along fault zones especially during heavy rains.

Geophysical methods can be applied in order to study the faults in an area. This has been done in Yogyakarta in Beijing, China where electrical resistivity sounding and borehole studies were applied (Rosyidi *et al.,* 2008). The findings of this study showed presence of severe building and geotechnical damage close to ground surface of the underground faults. Gravity, magnetic and seismic surveys conducted near Hobble Creek Canyon across a fault zone revealed a graben structure that was previously unknown at an area that had been proposed for housing development (Benson and Mustoe, 1995).

Gravity and magnetic data supplement each other well in locating and delineating concealed faults (Benson and Hash, 1998). The magnetic anomalies may be associated with mineral-bearing waters that flow along fault planes and gouges and deposit magnetic minerals, such as magnetite, hematite and limonite (Benson and Mustoe, 1991, 1995; Vincent, 2000). Low electrical resistivity is also expected in fractured rocks and along a fault zone and especially if the fault has saline water flowing along the fault plain or has trapped minerals or saline water in the fault gauge.

No geophysical studies have been done focusing on guiding the developers of Kiamunyi estate. The objective of this study therefore, was to map the faults and/or fractures using

electrical resistivity, gravity and magnetic methods by mapping regions with anomalies. To do this, three geophysical methods were employed to map the faults shown in Figure 2.2. These were gravity, magnetic and electrical resistivity methods.

1.2 Statement of the problem

The increase in population and development in Kiamunyi region attracted this geophysical investigation in the area. Buildings constructed on faulted basement are at a risk of cracking on the walls and worse still can suffer subsidence in case of an earthquake or heavy rains. This can lead to loss of lives and destruction of property in addition to landscape degradation. Geophysical investigation has not been carried out to map the faults and fractures in this region and advice the developers of the growing estate. In this study, the dc electrical resistivity method was employed to check for the vertical and horizontal variation of the electrical conductivity of the subsurface rocks. To check for the variation in density and magnetic intensity, the gravity and magnetic methods respectively were used.

1.3 Objectives

1.3.1 Broad objective

To investigate the presence and extent of faults and fractures in Kiamunyi area of Nakuru town, using Geophysical techniques.

1.3.2 Specific objectives

(i) To measure the vertical variation of the apparent electrical resistivity in the subsurface.
(ii) To determine the lateral variation in density, magnetic intensity and electrical resistivity.
(iii) To compare the resistivity, gravity and magnetic methods in mapping of faults.

1.4 Hypothesis

(i) The apparent resistivity of the subsurface in the study area does not vary with depth.
(ii) There is no lateral variation in the density, magnetic and electrical resistivity of the rocks across faults in the study area.
(iii) The resistivity method does not give a better image of the subsurface to locate the faults as does the gravity and magnetic methods.

1.5 Justification

Kiamunyi area is one of the regions undergoing rapid development. This study showed a fault zone which if active should be avoided during infrastructural development. Reinforcing the basement with strong metals and concrete can also be practised in case the mapped fault is inactive. Buildings constructed on active faults can collapse especially during heavy rains or in case of an earthquake. Areas away from faults should therefore be potential areas for infrastructural development. To curb the water shortages in Kiamunyi region, exploration for water can be done along the mapped fault since faults mostly form paths where underground water flows. Hence, the mapped faults will guide future ground water surveyors in the region.

CHAPTER TWO

LITERATURE REVIEW

2.1 Geology of the study area

Kiamunyi lies at the foot of the Menengai volcano to the south west. The Menengai volcano is a major Quaternary caldera volcano and consists almost exclusively of strongly per-alkaline and Si-oversaturated trachytes (Leat, 1984; Simiyu and Keller, 2001; Wamalwa *et al*., 2013). It formed about 180 Ka (thousand years) as a trachyte lava shield volcano which collapsed at about 29 Ka to form a caldera after a large volume of magma was extruded from an underlying magma chamber (Leat, 1984; Mungania, 1999; Wamalwa *et al*., 2013). Rocks found in this region are mostly; phonolite, trachyphonolites, trachyte and minor tuffs that were emplaced in the region before the formation of the caldera (Wamalwa *et al*., 2013). The caldera lies on the floor of the Kenyan rift in the East African Rift. Its location is shown its location is shown in Figure 2.1.

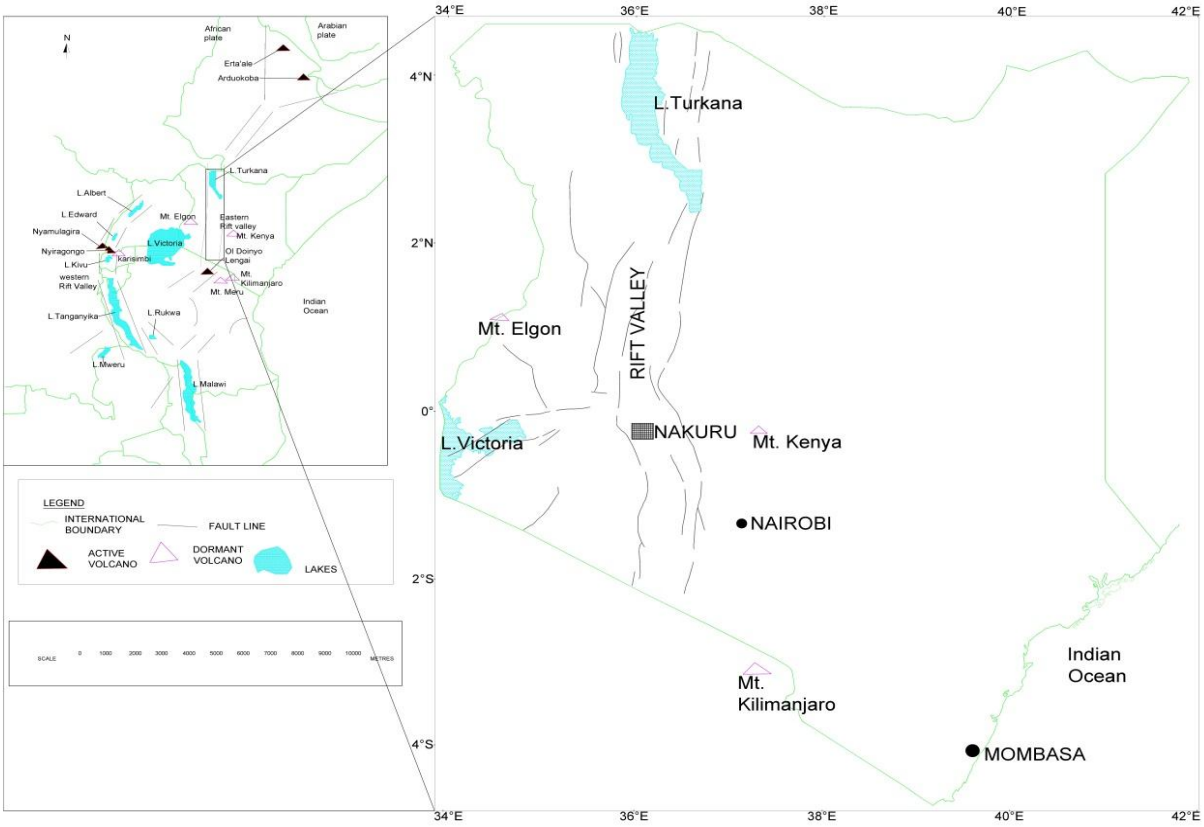

Figure **2.1**: Map of the Kenyan Rift in relation to the East African Rift.

The Menengai volcano is to the north of the area indicated by a rectangular box (Modified from Hormann, 2007)

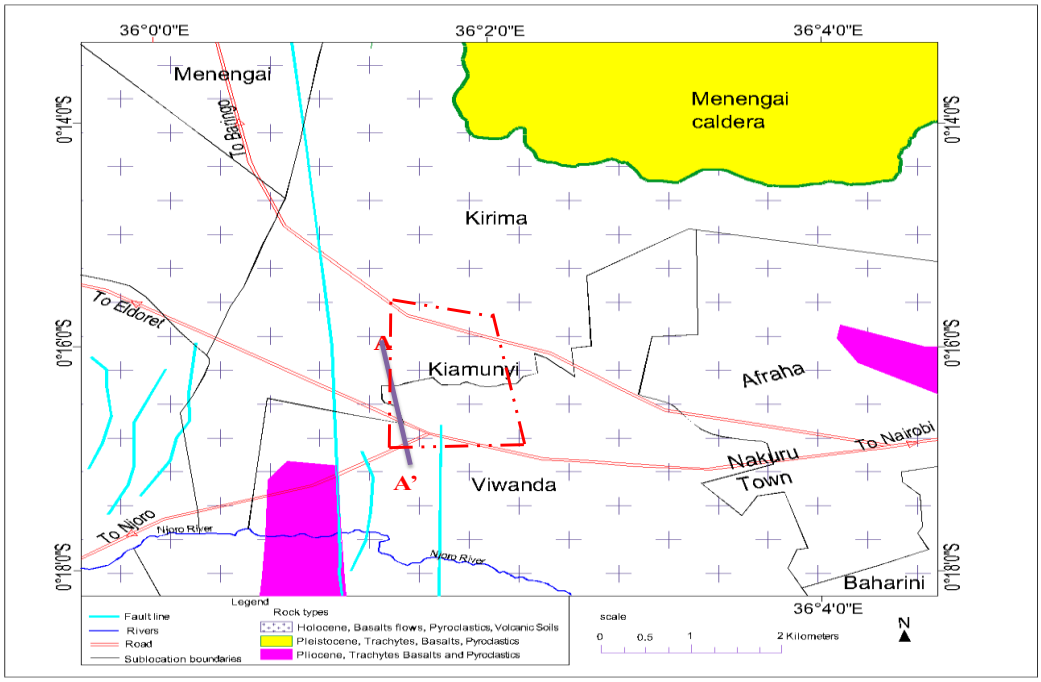

Figure **2.2**: Geological map of Nakuru area.

The region is located within the area indicated by a rectangular box in the map of the Kenya Rift; Figure 2.1 while the area of study is enclosed by the red dashed rectangle. (Modified from Bevcip, 1987).

2.2 Previous geophysical studies

Early geophysical investigations of the Kenya Rift utilized a different of methods to investigate deep crustal structure. Some of these methods include; seismic refraction profiles, local earthquake and teleseismic delay-time studies, gravity and geoelectric measurements (Swain *et al*., 1994). However, little has been done on individual volcanic systems (Wamalwa *et al*., 2013). By the middle 1980's a need was generally recognized for a detailed seismological investigation of the crust and sub-crustal lithosphere of the rift. Two major field investigations, KRISP-85 (Kenya Rift International Seismic Project 1985) and KRISP-90 were undertaken to meet this need (Prodehl *et al*., 1994a). KRISP experiments have provided most of the seismic data covering a big region of the Kenya Rift valley.

Geophysical studies conducted around the Menengai volcano are mostly aimed at determining potential sites for geothermal exploration and drilling sites for underground water. Detailed analysis of gravity and broadband magnetotelluric data in and around the volcano has been done (Wamalwa *et al*., 2013). The findings of this study were only favored geothermal exploration. From magnetic and gravity survey done in the Menengai geothermal field, the northern part of the geothermal field was observed to be demagnetized (Kemei *et al*., 2011). Seismic studies have been done in the area around Menengai volcano in exploration for geothermal resources (Young *et al*., 1991; Simiyu and Keller, 2001). Their findings indicated that most of the activity in the area is at a shallow depth with the region being served with a dense network of faults which help in recharging the geothermal reservoirs.

Detailed geophysical studies have however not been done around the Kiamunyi estate to investigate whether the studied faults cut across this region. This study therefore seeks to confirm the presence of the faults in Kamunyi estate that are shown on geological map of the area in Figure 2.2 by applying geophysical methods.

2.3.1 Electrical resistivity method theory

Electrical resistivity method measures or images subsurface electrical resistivity structures using direct or low frequency alternating current with a series of electrodes fixed into the ground. The electrical resistivity survey is based on the principle that the distribution of electrical potential in the ground around a current carrying electrode depends on the electrical resistivity and distribution of the surrounding soils and rocks. The electrodes consist of both current and potential electrodes for injecting the current into the ground and measuring the potential difference respectively. Apparent resistivity is the average resistivity of all soils and rock influencing the current (Telford *et al*., 1990).

The resistance R of a conducting cylindrical material such as the one shown in the Figure 2.3 is directly proportional to its length L and inversely proportional to its cross-sectional area *A*.

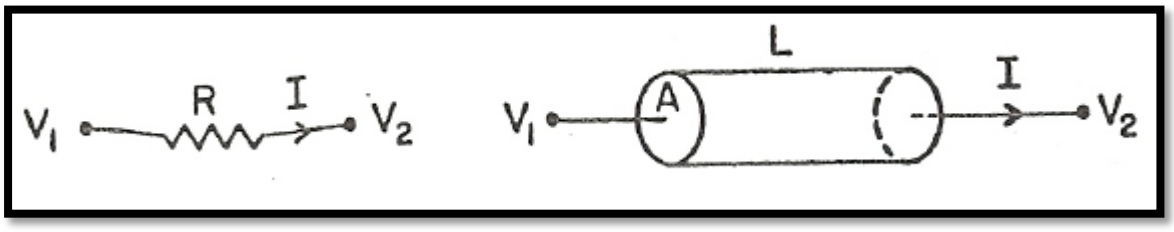

Figure **2.3**: Electrical conducting elements of the earth material

Implying:

$$R = \frac{\rho L}{A} \quad \text{(2.1)}$$

Where ρ is the electrical resistivity of the material; defined as the resistance in ohms between the opposite faces of a unit cube of the material. Hence:

$$\rho = \frac{RA}{L} \quad \text{(2.2)}$$

This is however only applied in simple homogeneous conductors. Apparent resistivity is calculated by dividing the measured potential difference by the input current and multiplying by a geometric factor which is specific to the array being used and electrode spacing (Telford *et al*., 1990).

Among the electrode arrays used in resistivity method is the Schlumberger electrode array. Here the potential electrodes M and N are placed at the center at a much smaller spacing as compared to the current electrodes A and B as shown in Figure 2.4.

The Geometric factor *K* calculated for the specific separation of the electrodes is given by

$$K = \left\{ \frac{2\pi}{\left\{ \frac{1}{AM} - \frac{1}{BM} - \frac{1}{AN} + \frac{1}{BN} \right\}} \right\} \quad \text{(2.3)}$$

Where *AM*, *BM*, *AN* and *BN* are distances between the current and potential electrodes.

The apparent resistivity ρ_a is given by.

$$\rho_a = K \frac{\Delta V}{I} \quad \text{(2.4)}$$

Where *I* is a known amount of current that is input into the ground. The potential difference ΔV between electrodes *M* and *N* can be calculated from;

$$\Delta V = \frac{I \rho_a}{2\pi} \left\{ \frac{1}{AM} - \frac{1}{BM} - \frac{1}{AN} + \frac{1}{BN} \right\} \quad \text{(2.5)}$$

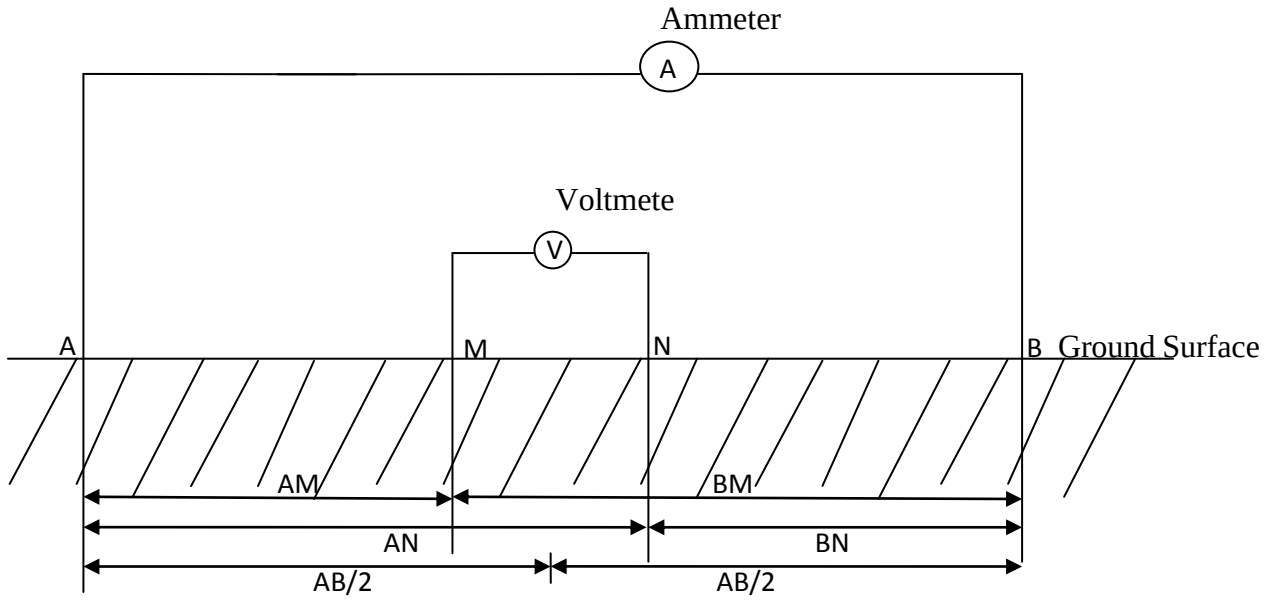

Figure **2.4**: Schlumberger electrode array (Modified from Sharma, 2002).

In Vertical Electrical Sounding, the electrode separation is increased from a fixed central position. In horizontal profiling, the current electrodes can be fixed at a large separation distance and the potential electrodes moved between the current electrodes as readings are being recorded. Alternatively the whole set up can be moved horizontally at some fixed electrode spacing as readings are made and recorded (McDowell, 1971). The electrical resistivity survey can be performed either on land or in water.

2.3.2 Gravity method theory

The basis of the gravity survey method is Newton's Law of Gravitation (Telford *et al*, 1990; Sharma, 2002). The force of attraction *F* between two masses m_1 and m_2, whose dimensions are small with respect to the distance *r* between them, is given by;

$$F = \frac{Gm_1m_2}{r^2} \quad \text{..... (2.6)}$$

Where *G* is the Gravitational Constant (6.67×10^{-11} m^3 kg^{-1} s^{-2})

The gravitational attraction of a spherical, non-rotating, homogeneous Earth of mass *M* and radius *R* on a small mass *m* on its surface is given as;

$$F = \frac{GM}{R^2}m = mg \quad \text{..... (2.7)}$$

The mass of the sphere acts as though it were concentrated at the centre of the sphere.

Force is related to the small mass by acceleration. The term $g = GM/R^2$ is known as the gravitational acceleration or gravity. The weight of the small mass is given by *mg* (Rivas, 2009).

On a spherical Earth, gravity would be constant. However, the Earth's ellipsoidal shape, rotation, irregular surface relief and internal mass distribution are the main causes of gravity variation over the surface of the earth (Telford *et al*., 1990).

There is a wide range in density among rock types, and therefore conclusions can be made about the distribution of rocks strata. Since faults are commonly adjacent to rocks of differing densities, then gravity method is therefore a good fault mapping choice (Rivas, 2009).

The variations in gravity can be due to lateral changes in the density of the subsurface rocks in the vicinity of the measuring point. Density variations can be very small and uniform at times, therefore the gravimeters are usually very sensitive so as to measure one part in 100 million of the earth's gravity field (980 Gals or 980,000 mGals) in units of mGals or μGals (Telford *et al*., 1990; Sharma; 2002; Mariita and Keller, 2007). The subsurface geology is usually investigated on the basis of variations in the Earth's gravitational field arising from differences of density between subsurface rocks. An underlying concept is the idea of a causative body, which is a rock unit of different density from its surrounding. This may represent a subsurface zone of anomalous mass and causes a localized perturbation in the gravitational field known as gravity anomaly. Buried features on a bedrock surface, such as a buried valley, fault, can give rise to measurable anomalies.

The method however, is limited by ambiguity and the assumption of homogeneity. A small mass distribution at a shallow depth can produce an effect similar to a large mass at depth. Therefore, if a second geophysical method is used a better conclusion can be arrived at. Gravity surveys can be carried on land, in marine areas as well as from an aircraft (Telford *et al*., 1990).

Gravity surveying is sensitive to variations in rock density; therefore, an appreciation of the factors that affect density aid's the interpretation of gravity data. Gravimeters do not give direct measurements of gravity. A meter reading is taken which is then multiplied by an instrumental calibration factor to produce a value of observed gravity (g_{obs}). The correction process is known as gravity data reduction or reduction to the geoid.

The corrections applied are;

i) Instrument drift*:* Gravimeter readings change (drift) with time as a result of elastic creep in the springs, producing an apparent change in gravity at a given station. The instrumental drift is determined by repeating measurements at the same stations at different times of the day.

ii) Earth's tides*:* The solid earth responds to gravitational pull of the Moon, and to a lesser extent of the Sun, this is known as the Earth tide (E_T). E_T gives rise to a change in gravity of up to three gravity units (g.u) with a minimum period of about 12 hours. Repeated measurements at the same stations permit estimation of the necessary correction for tidal effects over short intervals, in addition to determination of the instrumental drift for a gravimeter.

iii) Observed gravity *(g_{obs}):* This is the Gravity reading observed at each gravity station after corrections have been applied for instrument drift and earth tides.

iv) Latitude correction *(g_n):* Correction subtracted from g_{obs} that accounts for Earth's elliptical shape and rotation. The gravity value that would be observed if Earth were a perfect (no geologic or topographic complexities), rotating ellipsoid is referred to as the *normal gravity*.

$$gn = 978031.85\ (1.0 + 0.005278895\ sin^2(lat) + 0.000023462\ sin^4(lat))\ (mGal) \quad \text{.....(2.8)}$$

Where *lat* is latitude

v) Free-air correction *(g_{fa}):* The free-air correction accounts for gravity variations caused by elevation differences in the observation locations. The form of the free-air gravity anomaly, g_{fa} , is given by:

$$g_{fa} = g_{obs} - g_n + 0.3086h\ (mGal) \quad \text{……(2.9)}$$

Where *h* is the elevation (in m) at which the gravity station is above the datum or the sea level.

vi) Bouguer slab correction *(g_b):* The Bouguer correction is a first-order correction to account for the excess mass underlying observation points located at elevations higher than the elevation datum (sea level or the geoid). Conversely, it accounts for a mass deficiency at observation points located below the elevation datum. The form of the Bouguer gravity anomaly, g_b, is given by:

$$g_b = g_{obs} - g_n + 0.3086h - 0.04193\rho\ h\ (mGal) \quad \text{……(2.10)}$$

Where ρ is the average density of the rocks underlying the survey area.

vii) Terrain corrected bouguer gravity *(g_t):* The terrain correction accounts for variations in the observed gravitational acceleration caused by variations in topography near

each observation point. Because of the assumptions made during the Bouguer Slab correction, the terrain correction is positive regardless of whether the local topography consists of a mountain or a valley. The form of the Terrain corrected,

Bouguer gravity anomaly, g_t, is given by:

$$g_t = g_{obs} - g_n + 0.3086h - 0.04193\,\rho\,h + TC\ (mGal) \quad \text{.....(2.11)}$$

Where *TC* is the value of the computed terrain correction.

Assuming these corrections have accurately accounted for the variations in gravitational acceleration they were intended to account for, any remaining variations in the gravitational acceleration associated with the terrain corrected Bouguer gravity is assumed to be caused by a geologic structure (Telford *et al*., 1990; Rivas, 2009).

2.3.3 Magnetic method theory

Magnetic field anomalies arise as a result of the magnetization of crustal rocks which are under the constant influence of the Earth's magnetic field. Magnetic method involves mapping variations in the magnetic field to determine the location, size, and shape of such bodies (Telford *et al*., 1990; Sharma, 2002). Detection depends on the amount of magnetic material present and its distance from the sensor. Bodies that are shallow with magnetic elements are easily detected as compared to bodies that are deep and with less magnetite.

The aim of a magnetic survey is to investigate subsurface geology on the basis of anomalies in the Earth's magnetic field resulting from the magnetic properties of the underlying rocks.

Within the vicinity of a bar magnet a magnetic flux is developed which flows from one end of the magnet to the other. This flux can be mapped from the directions assumed by a small compass needle suspended within it. The points within the magnet where the flux converges are known as the poles of the magnet (Telford *et al.*, 1990).

The force *F* between two magnetic poles of strengths p_1 and p_2 separated by a distance *r* is given by,

$$F = \frac{\mu_{\circ} p_1 p_2}{4\pi\mu_R r^2} \quad \text{..... (2.12)}$$

Where $\mu_{\circ}$ and μ_R are constants corresponding to the magnetic permeability of vacuum and the relative magnetic permeability of the medium separating the poles. The force is attractive if the poles are of different sign and repulsive if they are of like sign.

The magnetic field *B* due to a pole of strength *p* at a distance *r* from the pole is defined as the force exerted on a unit positive pole at that point.

$$B = \frac{\mu_{\circ} p}{4\pi\mu_R r^2} \quad \text{..... (2.13)}$$

For a single pole of strength *p*, the magnetic potential *V* at a distance *r* from the pole is given by

$$V = \frac{\mu_{\circ} p}{4\pi\mu_R r} \quad \text{..... (2.14)}$$

The magnetic field component in any direction is then given by the partial derivative of the potential in that direction (Reilly, 1972).

The magnetic data should be corrected for diurnal variations. This is usually added or subtracted to the field reading depending on the readings at the base station at that specific time (Rivas, 2009). Magnetic survey data is usually displayed as individual profiles or as contour maps.

CHAPTER THREE

MATERIALS AND METHODS

3.1. The study area

Kiamunyi lies to the south west of Menengai volcano and is one of the estates of Nakuru town to the west of the town. It is at an altitude of about 1,859 m above sea level and bounded by latitudes 9968200 m and 9970200 m to the south and north respectively and longitudes 168800 m and 171000 m to the west and east respectively.

The area is covered by sediments derived from the erosion of Tertiary-Quartenary volcanic rock suits (Baker, 1986; Kagasi *et al*., 1988). Kiamunyi has surface depressions which are seen as surface fault scarps. The area studied measured about 5 square kilometers

3.2 Electrical Resistivity Method

Most rocks conduct electricity by electrolytic rather than electronic processes. Porosity is therefore the major control of the resistivity of rocks, and resistivity generally decreases as porosity increases. Crystalline rocks with negligible intergranular porosity are conductive along cracks and fissures.

3.2.1 Vertical Electrical Sounding data collection

To investigate changes in resistivity with depth, the electrodes spacing is usually increased after each measurement. This is referred to as Vertical Electrical Sounding (VES). For this study, a total of five soundings (VES-1 – VES-5) at randomly selected stations were done to cover the whole study area. Stations were selected on the basis of ease of accessibility and the availability of space that could allow up to 500 m which was the maximum current electrode separation used. The instrument used for this survey was the ABEM Signal Averaging System, (SAS 1000) Terrameter.

The electrodes *A, B, M* and *N* were driven into the ground to a depth of about 30 cm using a hammer. The minimum half current electrodes and potential electrodes separation measured from the centre of the configuration (the station) were 1.6 m and 0.5 m respectively. The current and potential difference for the specific electrode separation as displayed on the digital readout screen of the equipment were read and recorded in the field notebook. The electrode separations were shifted after each reading. A maximum separation of up to *AB/2* and *MN/2* of 250 m and 25 m respectively was used. The shifting of the electrodes was

guided by the decades covered. Eight readings were taken for the decade 1 m to 10 m and 9 readings for the decade 10 m to 100 m. This procedure was then repeated for the five soundings.

3.2.2 Horizontal Electrical Profiling data collection

To investigate lateral changes in apparent resistivity or localised anomalous features an array with constant spacing was used. Two horizontal electrical profiles were done in an orientation treading West-East. This would help in determining areas with lateral apparent resistivity variations. The West-East orientation ensured that the profiles cut almost perpendicular to the probable geological structure. The potential and current electrodes separations were maintained as 20 m and 100 m respectively. Hence a depth of around 30 m was surveyed. This separation was arrived at after analyzing the vertical electrical sounding data. A depth with consolidated rocks was the target in this case; either the weathered or the partly weathered layer. Each station location was recorded alongside the measured voltage and injected current. This was used in calculating the apparent resistivity for each station along the profiles using equations 2.3 and 2.4. After each reading the whole set up was moved to another station 10 m away along the profile. Constant inter station separations of 10 m were maintained throughout. This is because the anticipated fault zone is likely more than 10 m wide. Hence an inter-station separation of 10 m would most likely hit the anticipated fault.

3.3 Gravity data collection

The La Coste and Romberg gravimeter was used for the gravity data collection. Stations were located at least 100 m from known sources of vibrations such as the busy Nakuru-Eldoret and Nakuru-Baringo roads to minimize the effects of vibrations caused by moving vehicles. This was necessary because the equipment is sensitive to vibrations.

Gravity measurements were taken at random stations making sure to cross the anticipated fault with an inter-station separation of 30 to 50 m. A station away from sources of vibrations in the study area was established to act as a temporary base station. Readings were taken at the base station before commencing the day's work and after the day's work. Station coordinates and elevations were determined using Garmin 72 GPS which has an accuracy of 0.5 m. The values were recorded alongside the meter readings. The station elevation would be needed to compute the Bouguer slab correction. The maximum error in determining the elevation of each station did not exceed 0.5 m as read from the GPS. Hammer's method was

employed to obtain the terrain corrections. This was done by dividing the region around each station into three concentric rings of radius 2 m, 20 m and 50 m. The mean difference in elevation between the station and each segment was then determined at angular intervals of about 90^0, 45^0, and 22.5^0 from the inner segment to the outer segment respectively (Sharma, 2002). The Hammer Chart was then used to deduce the terrain correction for each station.

3.4 Magnetic data collection

Establishing and positioning of magnetic stations including the base station was done using a hand held GPS. Two Geometrics 856 Proton Precession Magnetometers were used for this study. The proton precession magnetometer measures the absolute values of total magnetic field intensity to a resolution of 0.1nT. To minimize data errors caused by the magnetometer operator, it was ensured that the magnetometer operator did not carry any metallic object. For this reason the station coordinates were taken first using the GPS after which the magnetometer reading was taken. Hence the GPS and the magnetometer were not used simultaneously. The sensor (measuring element) for the base magnetometer and that used for the field data collection were mounted on four and two stands respectively. This was to ensure that the sensors were relatively far from the ground and the observer in order to remove them from potential sources of noise present close to the ground (Parasnis, 1979; Telford *et al*., 1990).

A base station, far from power lines and metallic objects was chosen.

Figure **4.1**: G-856 magnetometer set to take readings at the base station

The base magnetometer was set to take and store readings at the base station for the whole day during a data collection exercise. Along with the magnetic field readings, the base magnetometer was also set to store the time when each reading was taken. This was to be used in correcting for diurnal variations (Parasnis, 1979; Rivas 2009).

Stations were randomly selected at inter-station spacing of about 30 to 50 m. However the fact that the study area is already occupied posed a major problem of magnetic noise in the region, and hence magnetic data collection from some of the areas was impossible. For instance the dense network of power lines was a hindrance to continuous data collection. Possible sources of magnetic noise were therefore avoided by locating the stations at least 50 to 100 m away from them. The magnetometer was set to take three readings at each station and display the average value. A total of three hundred and sixty five (365) stations were occupied in a period of four days. Coordinates of the stations were taken using the hand held GPS. The time when a specific reading was taken, was recorded alongside the average field reading and coordinates of the station. This was to be used for the diurnal corrections.

CHAPTER FOUR

RESULTS AND DISCUSSIONS

4.1.1 Vertical Electrical Sounding data

The geometrical factor, K was calculated for the electrode spacing by applying equation 2.3. Equation 2.4 was then applied to calculate the apparent resistivity values (ρ_a). The apparent resistivity values were then plotted against the half current electrode separations on a log-log scale to obtain VES sounding curves. These curves are shown in Figure 4.1 (*a-e*)

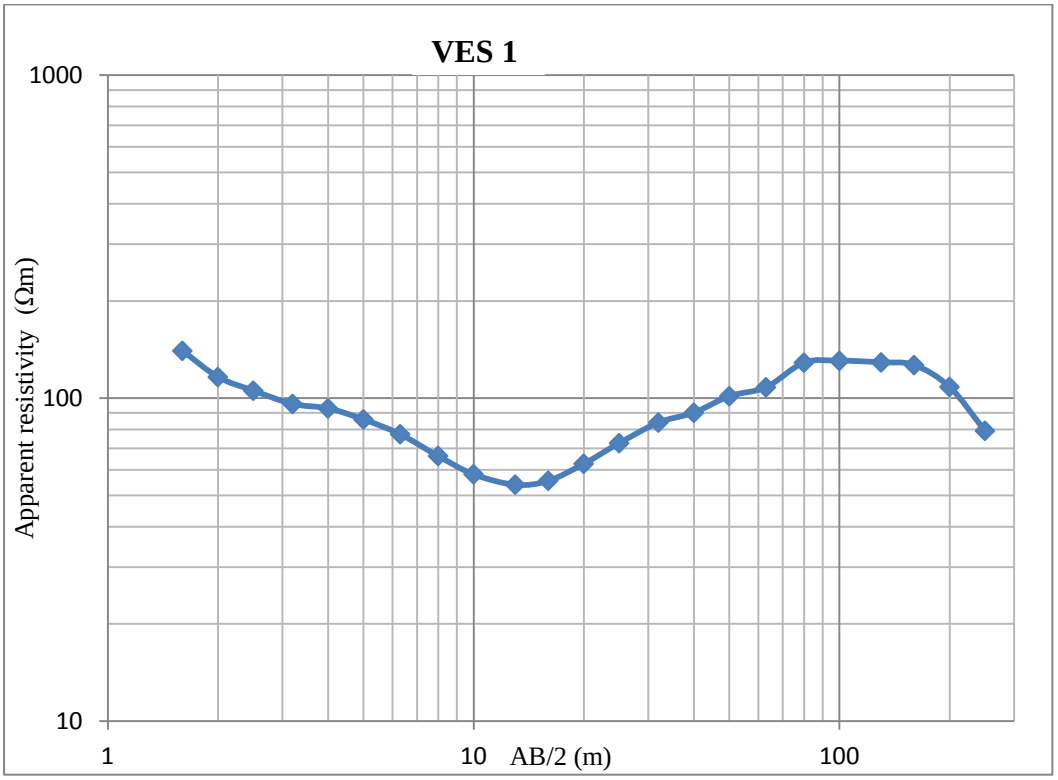

(a)

VES station **1.** Location: (UTM 37 S 0170078, 9969216)

Elevation: 1895 *m*

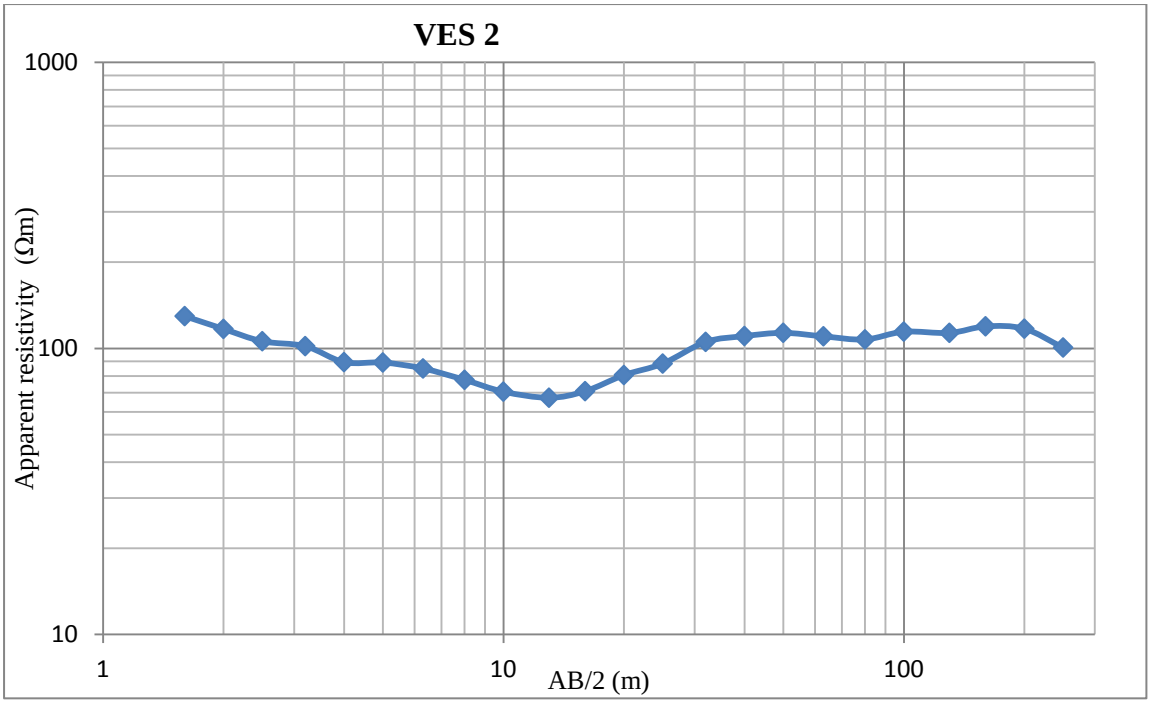

(b)

VES station **2.** Location: (UTM 37 S 0170078, 9969216)

Elevation: 1895 *m*

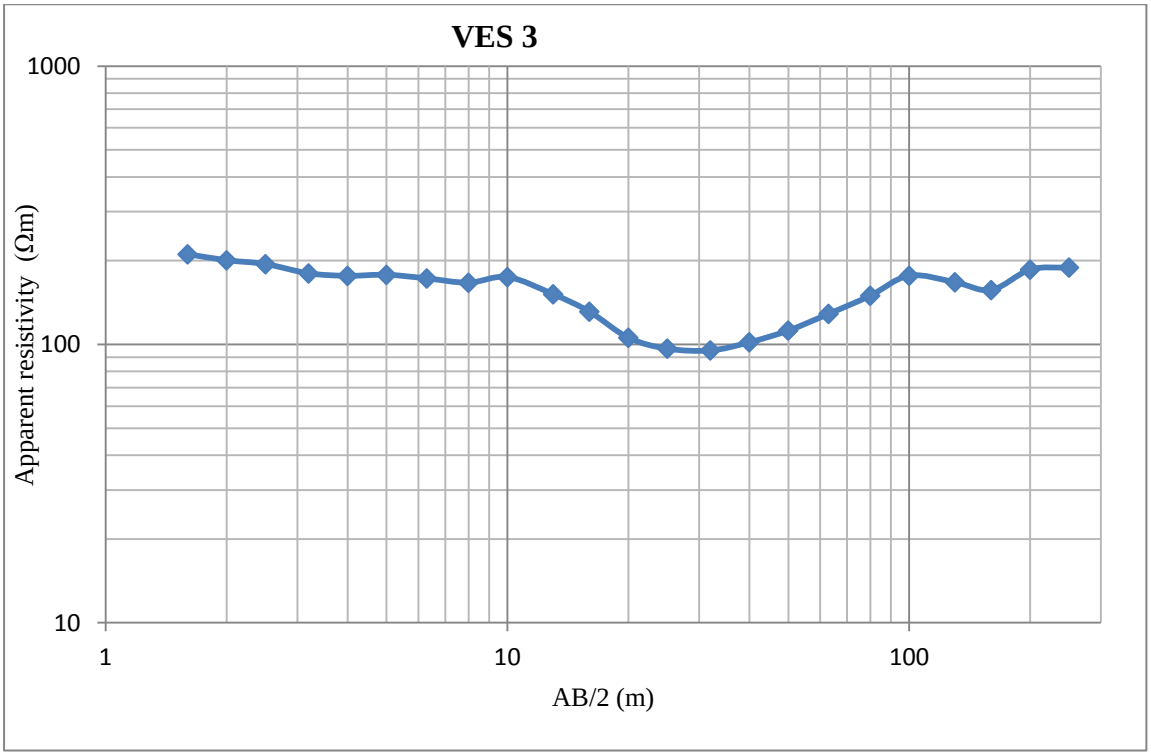

(c)

VES station **3.** Location: (37 S 0170627, UTM 9968990)

Elevation: 1869 *m*

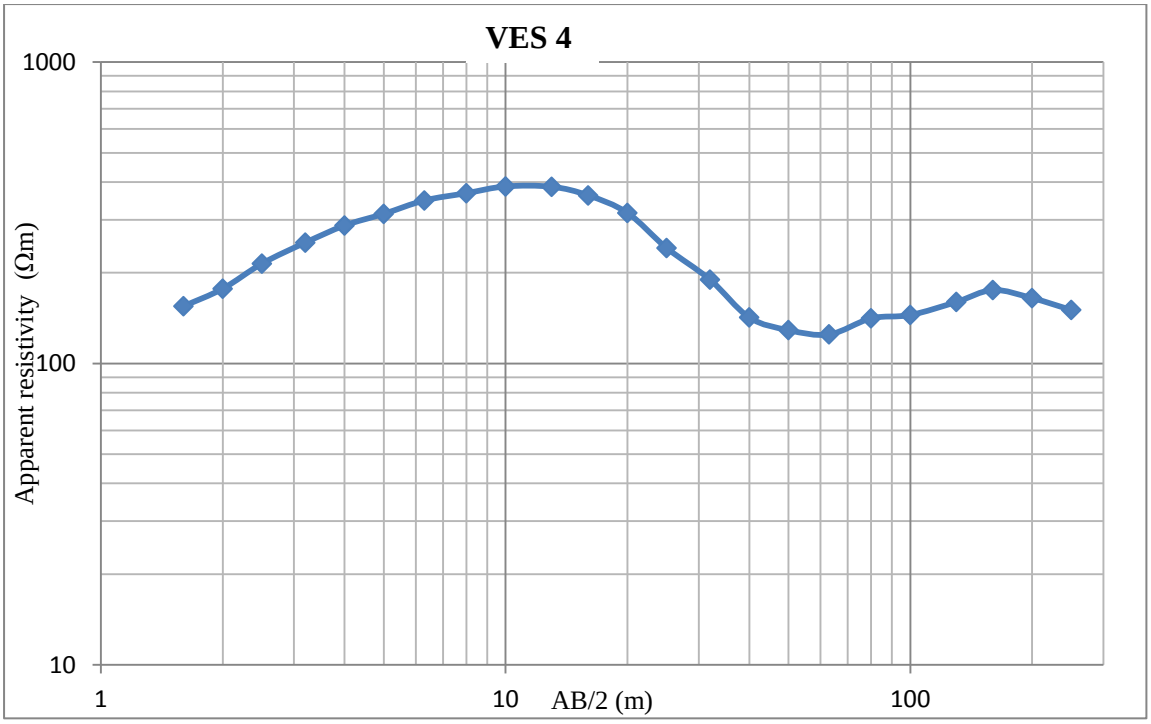

(d)

VES station **4.** Location: (37 S 0170183, UTM 9969428)

Elevation: 1905 *m*

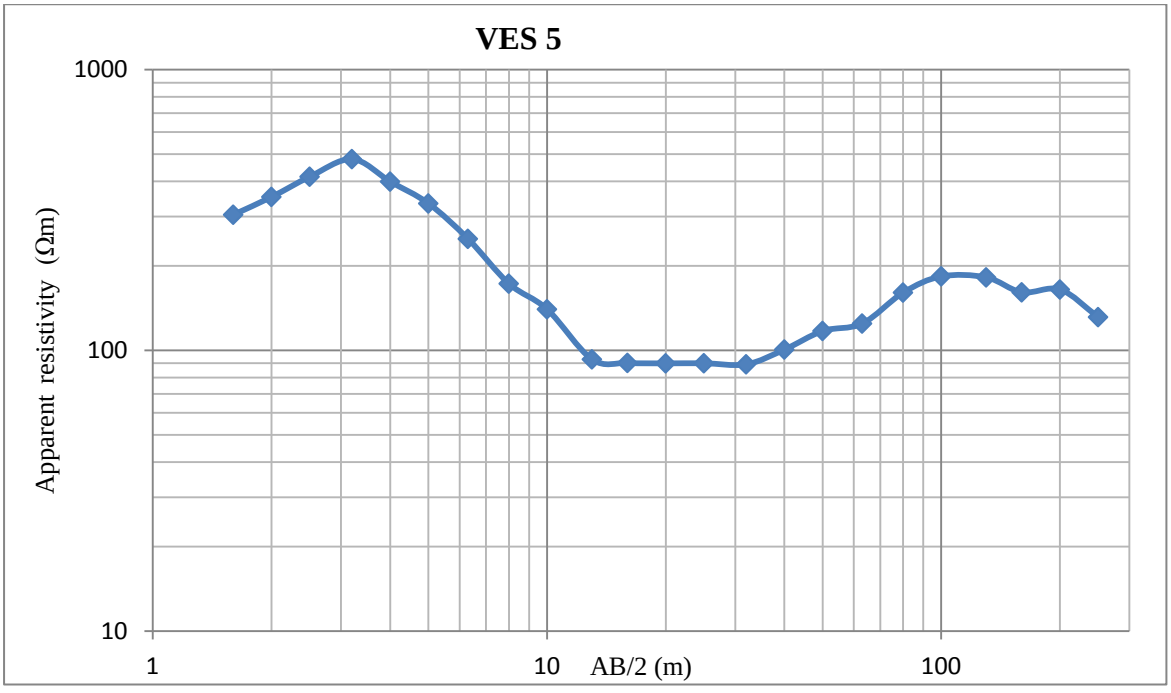

(e)

VES station **5.** Location: (37 S 0170124, UTM 9968302)

Elevation: 1864 *m*

Figure **4.1 (*a*-*e*)**: Plots of apparent resistivity against half current electrode separation.

The values plotted on the X-axis in the five curves are the depths surveyed from the surface. The curves for VES 1, VES 2 and VES 3 are similar in that they all start with a high apparent resistivity which then decreases to some minimum value.

In VES 1 the apparent resistivity decreases from the surface to a depth of 17.71 m. The average apparent resistivity for this layer is 79 Ωm. This resistivity then increases to an average apparent resistivity of 147 Ωm at a depth of 136.41 m. The apparent resistivity then decreases to about 72 Ωm towards the basement.

In VES 2, the first layer has an average apparent resistivity of 88 Ωm which decreases to a depth of 17.70 m. It reaches a minimum at 17.80 m and then starts increasing to an average of 132 Ωm at a depth of 108.65 m. This further increases to 137 Ωm at a depth of 160 m. The basement has an average resistivity of 100 Ωm.

The first layer in VES 3 has an average apparent resistivity of 192 Ωm with a thickness of 6.9 m making it the thinnest first layer in the five soundings. This resistivity further decreases to 69 Ωm at a depth of 27.20 m. At a depth of 89.69 m the apparent resistivity increases to an average of 331 Ωm and then decreases to 168 Ωm at a depth of 160 m. The basement has an average apparent resistivity of 188 Ωm.

VES 4 and VES 5 are similar in that the apparent resistivity of their first layers are the highest and increases with depth. The apparent resistivity and layer thickness of VES 4 and VES 5 are 287 Ωm and 15.63 m and 418 Ωm and 3.23 m respectively. In both, the apparent resistivity decreases with an average resistivity of 108 Ωm and 70 Ωm at a depth of 72.65 m and 20.84 m for VES 4 and VES 5 respectively. This then increases to 102 Ωm and 261 Ωm at depths of 103.16 m and 134.86 m for VES 4 and VES 5 respectively. Towards the basement the apparent resistivity decreases to an average of 150 Ωm in VES 4 and 131 Ωm in VES 5.

The five VES curves revealed the heterogeneous nature of the subsurface. The geological layers beneath the study area are composed of top soil, weathered layer, partly weathered layer and the basement. The top soil has apparent resistivity values ranging from 79 Ωm to 418 Ωm and thickness varying from 3 m to 17 m. The weathered layer has apparent resistivity ranging between 69 Ωm and 147 Ωm and a depth of 20 m to 108 m. This layer is likely to be having a high moisture content which might be causing the low resistivity while the partly weathered layer has apparent resistivity values ranging from 102 Ωm to 331 Ωm at

a depth of 103 m to 134 m. A region with igneous felsic rocks with a resistivity of about 72 Ωm to 188 Ωm is also observed.

Analysis of the VES data helped in determining the electrode separation and hence the depth of probe of the horizontal electrical profiling. The depth to the second layer was concluded to be at 20 m to 108 m. If there are faults in the study region, then this is the layer that is likely to be faulted. A depth of 30 m was therefore ideal for the horizontal electrical profiling to make sure that the lateral variation apparent resistivity at this depth was studied.

4.1.2 Horizontal Electrical Profiling data

The horizontal resistivity profiles data was presented as an resistivity contour map.

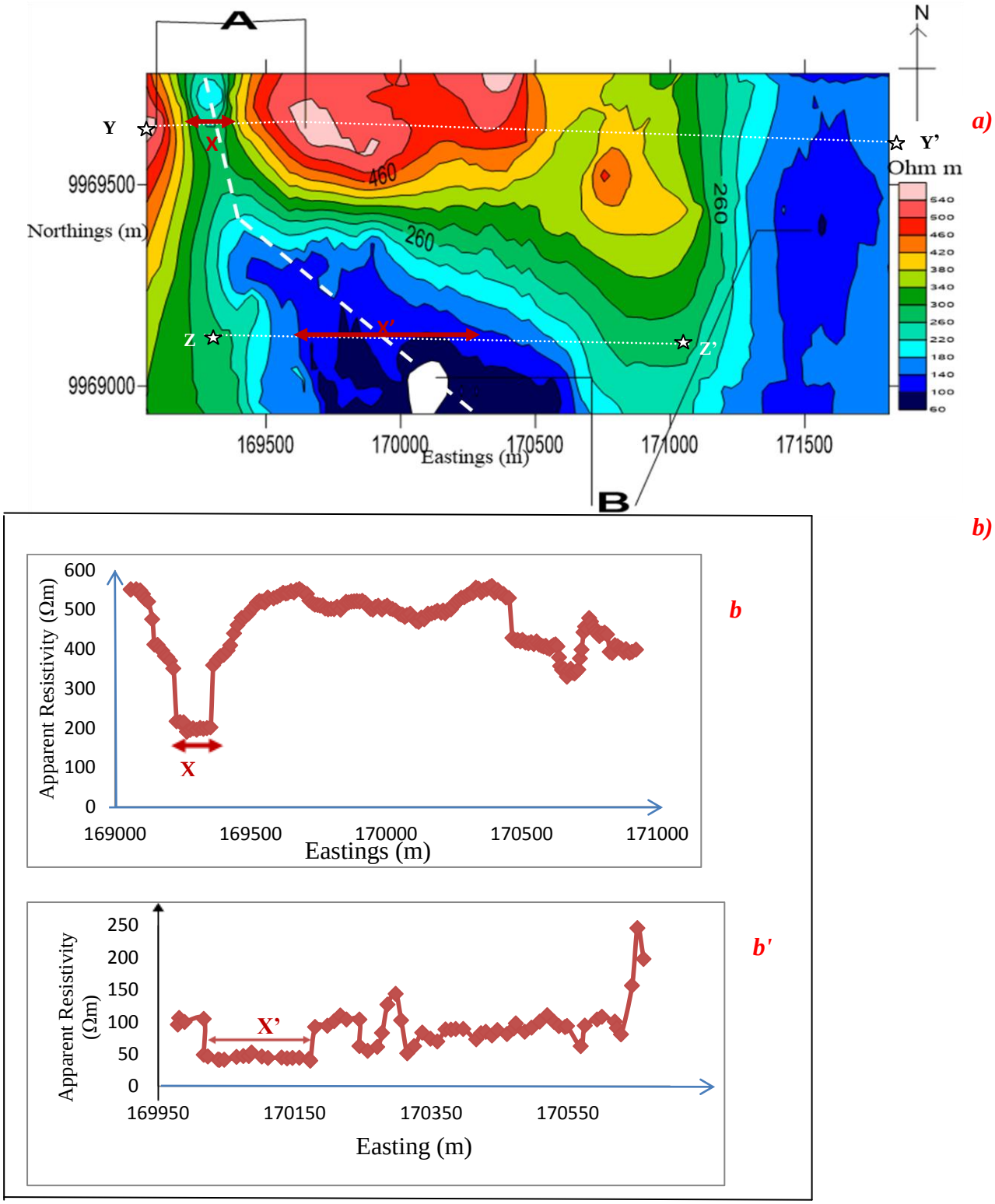

Figure **4.2**: ***a)*** Contour plot representing the resistivity profiling data with the mapped fault is shown in a white dashed line and ***b)*** apparent resistivity profiles

In the contour map, the region of highest resistivity is to the north with a resistivity of 540 Ωm while the lowest resistivity is to the south and has resistivity of 60 Ωm. All other apparent resistivity lies between these two values. Letters A and B shows areas of high and low resistivity respectively. High apparent resistivity areas are therefore seen on the areas to the northern and western side of this map while low resistivity areas are seen on the southern as well as on the eastern side of the map. A relatively low resistivity area is sandwiched between two high resistivity regions on the western side. The sandwiched area also has steep contours and seems to be linear running from north to south. The low resistivity region observed on the eastern and the southern parts of the contour map may imply areas with less compact rocks or rocks that are highly weathered as compared to the surrounding rocks. The highs to the north are presumed to be as a result of the rocks observed in the area.

The apparent resistivity profiles *b* and *b'* were also plotted. These were taken along the dotted lines labelled *Y-Y'*and *Z-Z'* in the contour map. The plotted profiles agree well with the trends in the contour map. The region of lowest resistivity in profile Y-Y' is labelled X and is shown on the contour map and on the profile. Similarly X' is also shown as the lowest resistivity region for profile Z-Z'. Both of these regions are observed between regions of relatively more resistive material. Region X' is observed to be wider and starts further to the east as compared to region X. Hence, if these low resistivity regions are anomalies caused by a fault, then it can be concluded that the fault stretches from Northwest to Southeast and widens towards the south. The high resistivity observed to the north of the contour map is suggested to be caused by the many igneous rocks observed in the area.

4.2 Gravity data

To obtain the Bouguer anomaly values, the various corrections to the gravity data were applied. These were; the drift correction, the free air correction referring to the ellipsoid, the Bouguer correction and the terrain correction (Sharma, 2002). The Bouguer correction was obtained using the formula:

$$g_B\ (mGal)\ = 0.4192 \times h \times \frac{2670}{10{,}000} \quad \text{..... (4.1)}$$

A constant rock reduction density of 2.67 g/cm^3 was assumed. Where g_B is the Bouguer correction in mGal and h is elevation in meters and 0.4192 = 2πG in which G = 6.67×10^{-11} m^{3}kg^{-1}s^{-2} is the gravitational constant (Parasnis, 1979; Telford *et al.*, 1990). This correction compensates for the mass between the station and the mean sea level which tends to reduce

the gravity value at an observation station (Telford *et al.*, 1990; Sharma, 2002). The Bouguer correction was added to the observed gravity value.

The free air correction was calculated using a constant elevation multiplication factor of 0.3086 mGal per metre (Telford *et al*., 1990):

$$g_{fa}\ (mGal) = 0.3086 \times h \quad \text{..... (4.2)}$$

Where g_{fa} is the free air correction in mGal and h is is the elevation in metres. The free air correction compensates for the reduction in gravity caused by increasing the distance from mean sea level. This correction was therefore added to the observed gravity value since all the stations were above the datum; which was assumed to be the sea level (Telford *et al.*, 1990; Sharma, 2002).

The terrain correction compensates for the effect of nearby topography. Terrain corrections were calculated radially outward from the concentric circles by applying the Hammer chart which applies equation 4.5 (Telford *et al.*, 1990).

$$g_T = G\rho\varphi\left\{(r_2 - r_1) + \sqrt{\mathrm{r1}^2 + (\Delta h)2} - \sqrt{\mathrm{r2}^2 + (\Delta h)2}\right\} \quad \text{..... (4.3)}$$

Where g_T is the terrain correction, φ is the angular intervals, Δh is the mean elevation between each segment and the gravity station, ρ is the density of the terrain material; taken to be 2.67 g/cm^3 and r_1 and r_2 are the radii of the inner and outer rings bounding the segments respectively. The terrain correction was subtracted from the observed gravity.

To minimize the instrumental errors caused by bumping or jarring the gravimeter, the meter was handled with care. Looping between few marked stations during the survey was also practiced to ensure that such errors were completely minimized and corrected. Slight instrumental and tidal drift were also minimized by looping back to the base station at the end of the day's work. For every station two readings were taken, whereby the average was calculated and recorded. This ensured that the random errors were kept to their minimum value. Based on tie points in the data set, maximum instrumental error and error due to drift were estimated to be 0.022 mGal. The terrain corrections were estimated to yield a total maximum error of 0.01 mGal. The maximum error in elevation difference determination was estimated to be 0.5 m. Consequently, the free air and Bouguer correction error for each station due to the error in elevation yielded a maximum error in gravity of 0.3086 mGal and 0.112 mGal respectively. Thus, the maximum error if all the above sources were to

accumulate would be at most 0.45 mGal. However, the possibility that all of these errors would accumulate with maximum value at any one station is not likely.

The gravity data was gridded to produce a simple Bouguer anomaly map of the study area with a constant contour interval of 10 mGal as in Figure 4.3.

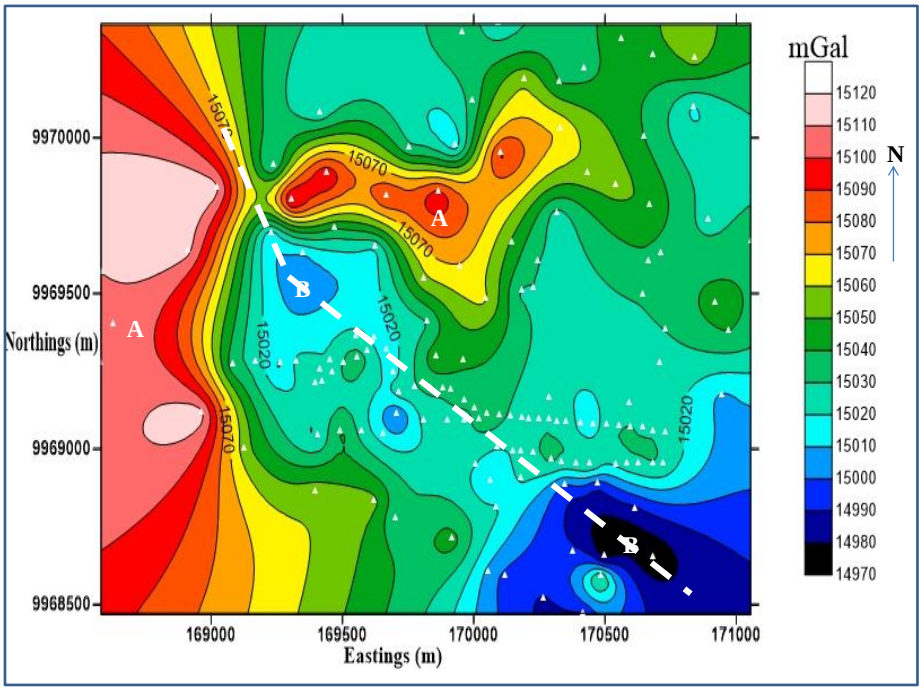

Figure **4.3**: Simple Bouguer-anomaly contour map of the study area; the mapped fault is shown in a white dashed line

The data stations are represented with white triangles. The different colour shades represents the gravity values in mGal with the highest and lowest gravity values in this area being 15120 mGal and 14970 mGal, marked with letters A and B respectively as read from the contour map.

Gravity highs appear on the west as well as the central regions of the map. This is the region marked A on the map while a gravity low marked B is observed on the south eastern side but stretches to the central parts of the study area. It is also observed that the contours are closely spaced and liner on the western side running from north to south.

4.3 Magnetic data

The major correction carried out on the absolute values of the total magnetic field was the diurnal corrections. To perform diurnal corrections, curves of the base magnetic field values

against time were plotted for every field day's base station data. These are shown in Figure 4.4. The curves obtained were used for the diurnal corrections where the first value on the curve was taken as the reference point. Depending on the base station reading at a specific time, the difference between the first base reading and the base reading at that specific time, was either added or subtracted to the field magnetic reading taken at the same time. The resulting field represented the relative values of the variation in total field strength with respect to the magnetic base station.

The field notes taken during data collection were used to counter check all the data points for possible interference. For this reason, some of the data points showing possibilities of noise were eliminated from the data set.

a)

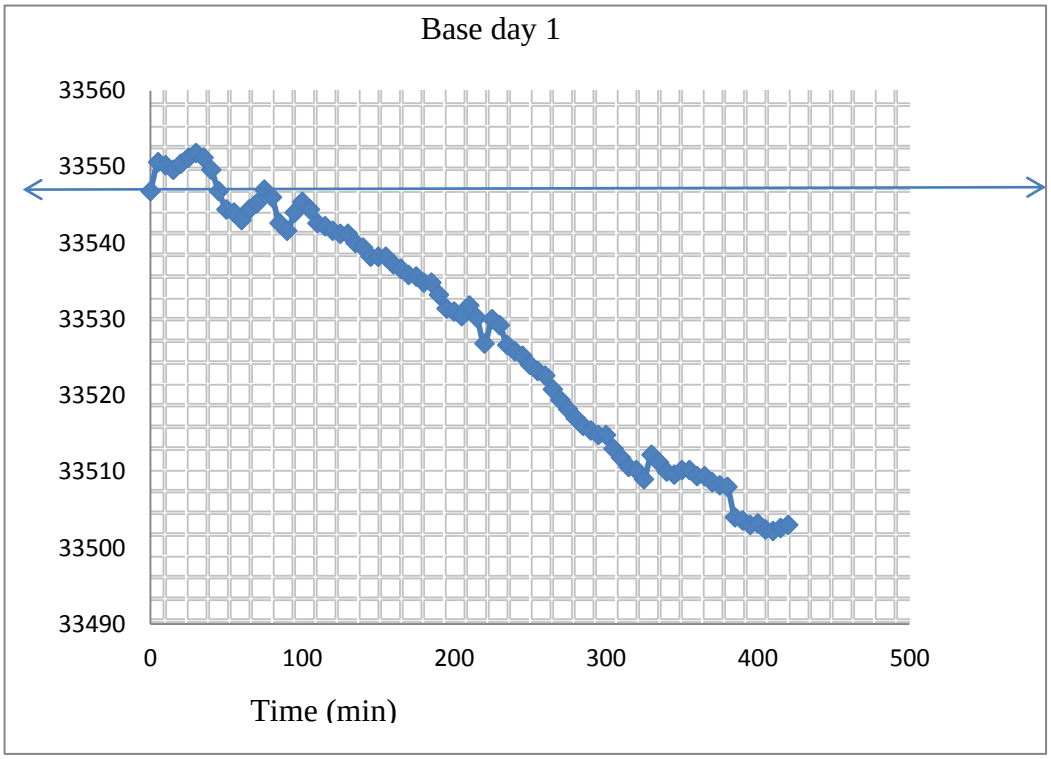

b)

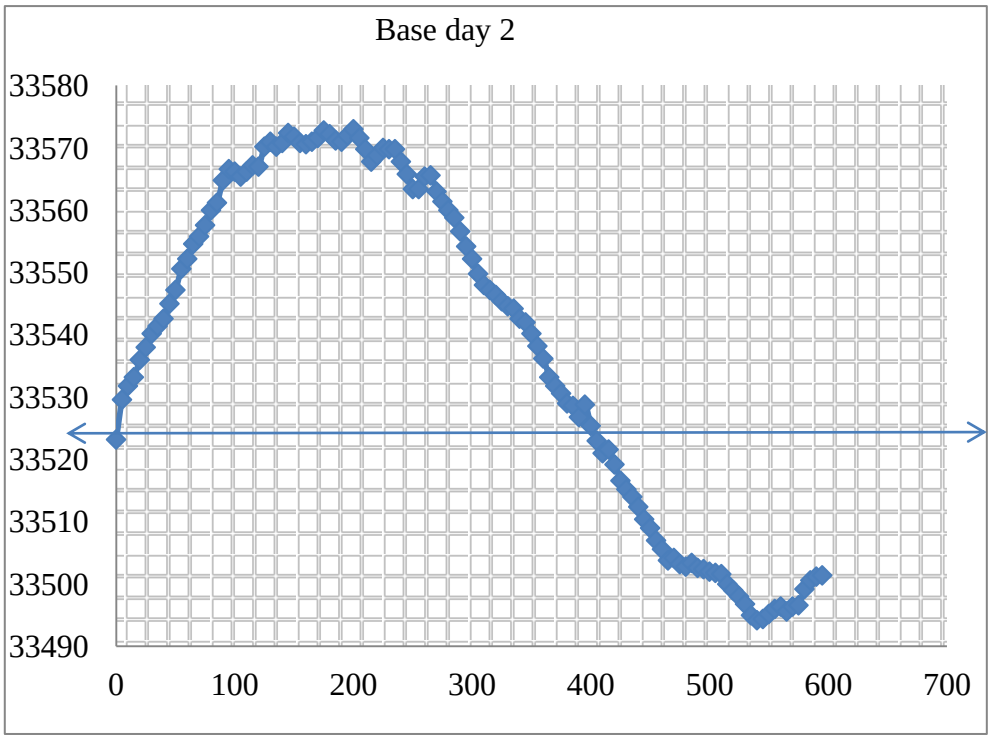

Field (nT)

Time (min)

c)

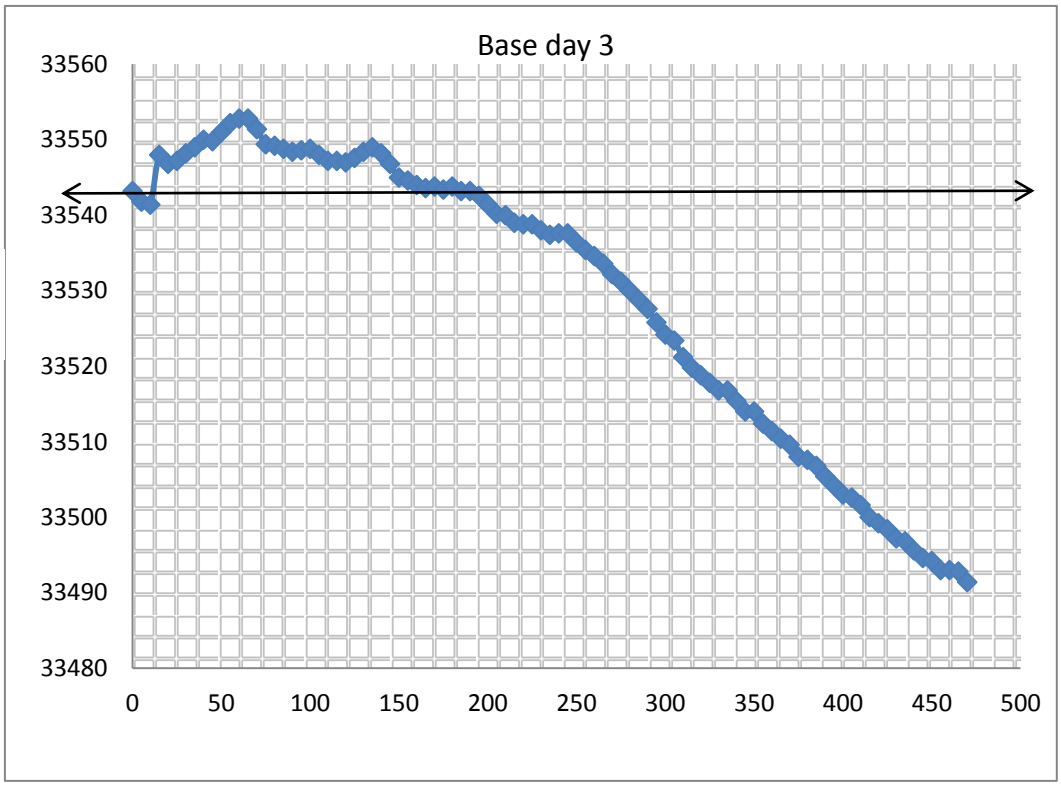

Field (nT)

Time (min)

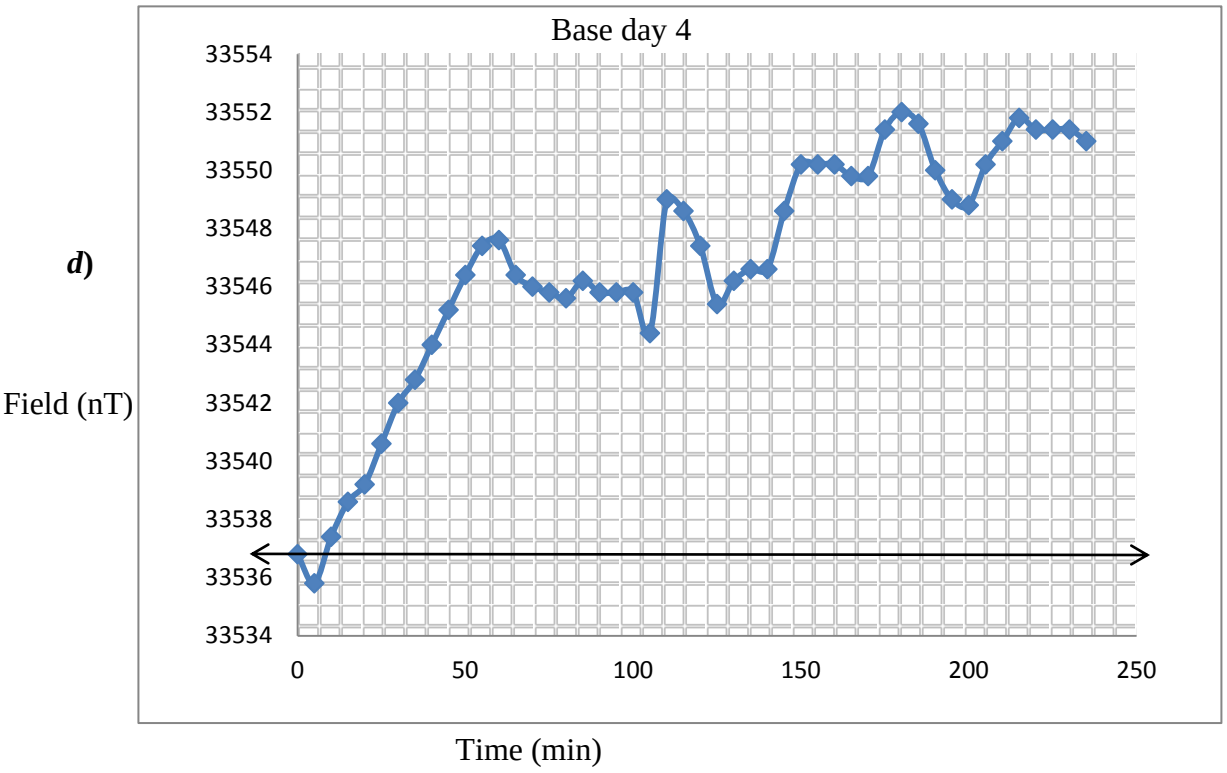

Figure **4.4** ***(a-d):*** Base station curves

The curves in Figure 4.4 (*a-b*) were plotted from each day's base station readings. As evident from the base station readings, the magnetic field of any specific station varies with time. These temporal variations are caused by particle and electromagnetic radiation from the sun perturbing the ionosphere of the earth and thus the geomagnetic field (Sharma, 2002) hence the reason for applying the diurnal corrections. Diurnal variations may last several hours to one day and causes variations of the Earth's magnetic field at a specific field with time (Riddihough, 1971).

After correcting for diurnal variations, a low pass filter 3(3X3) was applied to the data. This would ensure removal of the low wavelengths due to cultural noise.

The data was then gridded and a total magnetic field intensity contour map generated. A constant contour interval of 20 nT was used as shown in Figure 4.6.

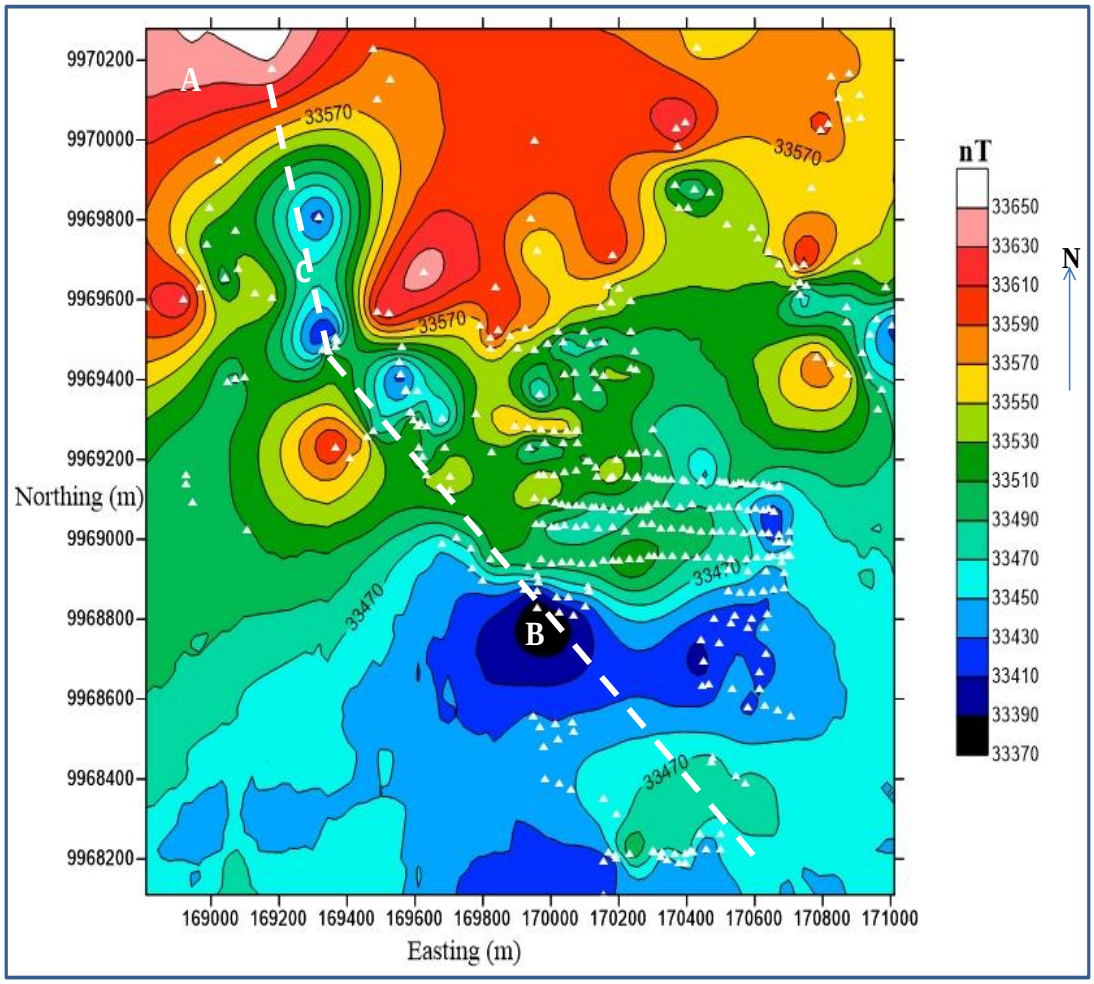

Figure **4.5** Total magnetic intensity contour map; the mapped fault is shown using the white dashed line.

As read from the magnetic intensity contour map, the highest magnetic intensity observed is around 33650 nT while the lowest magnetic intensity is 33370 nT. These are the regions marked A and B on the total magnetic intensity contour map respectively.

On the western side of the magnetic contour map, a low magnetic intensity region; labeled C is observed which stretches towards B. This low magnetic intensity region occurs between two high magnetic intensity regions. This region can be related to a linear structure such as a fault or a region of low magnetic materials.

CHAPTER FIVE

CONCLUSIONS AND RECOMMENDATIONS

5.1 Conclusions

i) It's observed from all the vertical electrical sounding curves that the apparent resistivity varies with depth in the region studied. Hence the near surface material in this region is non homogeneous

ii) A low resistivity region is observed from the horizontal electrical resistivity data when plotted both as profiles and when the apparent resistivity contour map is generated. Hence a lateral variation in apparent resistivity in the study area is observed. The relatively low resistivity region observed between high resistivity regions running from north to south in the resistivity contour map may be representing a fault zone. High gravity regions represent relatively denser rocks as compared to the adjacent rocks. On the other hand, low gravity regions show possible areas with less dense or unconsolidated rocks as compared to the surrounding. This might be an indication of a fractured or faulted zone. However, since the low gravity zones occur between high gravity zones, then this is likely to be caused by a fault. A lateral variation in gravity hence density is observed in the study area. A low magnetic intensity region occurring between high intensity zones is a possible indication of a fault zone; which is a distinct signature of faults. The low intensity is likely to be as a result of rocks that subsided during the formation of the fault zone. A lateral variation in magnetic intensity in the study area is also observed from the magnetic contour map. Generally, the electrical resistivity, magnetic field and density are seen to vary laterally across the fault zone. The region where all these variations are observed coincides with the surface trench like depression observed in the area. Hence it can be concluded that the observed trench is a fault zone that runs from Northwest to Southeast.

iii) The anomalies observed from all the three methods run Northwest-Southeast which agrees well with the previous studies done around the region which show that the faults in this area run north-south as seen in the geological maps of the study area shown in Figure 2.2 (Ngecu and Nyambok, 2000). This is the region cutting through point labelled A and A' in Figure 2.2. The three data sets show similar trends whereby the anomaly seems to cut Northwest-Southeast hence the general trend of the fault

mapped in this study. It is therefore concluded that a fault exists in the study region as shown in white dashed line in Figures 4.2 *a*, 4.3 and 4.5. The fault runs Northwest-Southeast and seems to originate from the Menengai volcano and terminate in Lake Nakuru. The three methods used in this study; electrical resistivity, gravity and magnetic methods all give an equal contribution to the mapping of this fault. A single method could also have given a sure conclusion in mapping the said fault. However, for a successful conclusion to be arrived at, it's important that at least two geophysical methods be used. Therefore, none of the three methods used was more effective than the others in mapping this fault zone. All that is required is to assess the applicability of each method to the problem at hand.

5.2 Recommendations

i) A fault zone was successfully mapped, but whether it is an active fault or not was not determined. It is therefore recommended that, seismic stations be set in the area to determine the activity of this fault. If observed to be active, then developed around the faulted zone should be discouraged. If inactive then precautionary measures like reinforcement can be employed.

ii) It is observed that the electrical, magnetic and gravity methods gave a similar trend in mapping this fault. Therefore, none of the three methods can be said to be a better fault mapping method. Its recommended that any two methods can be used in mapping a fault zone depending on their applicability

iii) More research should be done to map any other faults existing in the entire Kiamunyi region and all the outskirts of Nakuru town for safe expansion of the town in case there are any active faults.

REFERENCES

Ako A.O. and Olorunfemi M.O., (1989), Geoelectric survey for groundwater in the Newer Basalts of Vom Plateau State: *Nig Journal of Mining and Geology* 25 pp 247-450

Baker B. H., (1986), Tectonics and volcanism of the southern Kenya rift valley and its influence on rift sedimentation: *Geol Soc Spec* **24**, pp 45–57

Baker B.H., (1958), Geology of the Magadi area. Geological survey of Kenya Report 42: The Government printer, Nairobi.

Benson A.K. and Hash S.T., (1998), Integrated three dimensional interpretation of major concealed faults beneath Mapleton, Utah county, Utah using gravity data, supported with Magnetic data: *Engineering Geology*. **51**, 109-130.

Benson A.K. and Mustoe N.B., (1991), Delineating concealed faults and shallow subsurface geology along the Wasatch Front, Utah, USA, by integrating geophysical and trench data: *Quarterly Journal of Engineering Geology*, **24**, 375-387.

Benson A.K. and Mustoe N.B., (1995), Analyzing shallow faulting at a site in the Wasatch fault zone, Utah, USA by integrating seismic gravity, magnetic and trench data: *Engineering Geology*, **40**, 139-156.

Bevcip F., (1987), Ministry of energy regional development, Kenya

Hormann C., (2007), *Views of the Earth, Artificial Images of Our Real Planet: The Afar Triangle.* http://earth.imagico.de/view.php?site=ethiopia, Accessed on May 21, 2007.

Kagasi J., Ochieng J., Theuri F. and Mosley P., (1988) Geological hazard appraisal in the Nakuru area. Mines and Geological Department, Nairobi

Kemei J.K., Langat G.K., Ambusso W. and Okumu J., (2011), Results of Gravity and Ground Magnetic Survey of Menengai Geothermal Field, Kenya: Proceedings, Kenya Geothermal Conference 2011 Kenyatta International Conference Centre, Nairobi, November 21-22, 2011

Leat P. T., (1984), Geological evolution of the trachytic caldera volcano Menengai, Kenya rift valley: *Journal of the Geological Society*, **141**, 1057–1069.

Leat P.T., Macdonald R. and Smith R.L., (1984), Geochemical evolution of the Menengai caldera volcano, Kenya: *Journal of Geophysical Research*, **89**, 8571–8592.

Macdonald R., Navarro J.M., Upton B. and Davies G.R., (1994), Strong composition variation in peralkaline magma: Menengai, Kenya Rift Valley: *Journal of Volcanology and Geothermal Research*, **60**, 301–325,

Mariita N. O. and Keller G. R., (2007), An integrated geophysical study of the northern Kenya rift: *Journal of African Earth Sciences*, **48**, 80–94.

Mariita N. O., (2007), The gravity method: Presented at Short Course II on Surface Exploration for Geothermal Resources, organized by UNU-GTP and KenGen, 2-17 November, 2007.

McCall G.J.H., (1957), Geology and groundwater conditions in the Nakuru area: Technical Representation 3. Ministry of Works, Nairobi.

Mibei G. and Lagat J., (2011), Structural Controls In Menengai Geothermal Field Proceedings, Kenya Geothermal Conference 2011 Kenyatta International Conference Centre, Nairobi, November 21-22, 2011.

Mungania J., (1999), Overview of the geology of Menengai volcanic complex: Kenya Electricity Generating Company, Internal report.

Ngecu W. M. and Nyambok I.O., (2000), Ground subsidence and its socio-economic implications on the population-a case study of the Nakuru area in Central Rift Valley, Kenya: Environmental Geology, **39**, No. 6, pp. 567-574.

Omenda P. A., Opondo K., Lagat J., Mungania J., Mariita O., Onacha S., Wetangula G. and Ouma G., (2000), Ranking of geothermal prospects in the Kenya rift: Kenya Electricity Generating Company Limited, Internal report.

Orlando P. R., (1988), Interpretation of resistivity sounding from San Ignacio, Honduras: Geothermal Training Programme Reykjavic-Iceland Report 6.

Parasnis, D. S. 1979. Principles ofApplied Geophysics. 275 Chapman and Hall.

Prodehl C., Keller G.R. and Khan M.A., (1994a), Crustal and Upper Mantle Structure of the Kenya Rift: *Tectonophysics* **236**, 483p.

Reilly W.I., (1972), Use of the International System of Units (SI) in geophysical publications N.Z.J. Geol. *Geophysics*, **15**, 148–58.

Riddihough R. P. (1971), Diurnal Corrections to Magnetic Survey; An accessment of Errors, *Geophysical Prospecting* **19**: 788-803.

Rivas J., (2009), Gravity and Magnetic methods: Presentation on "Short Course on Surface Exploration for Geothermal Resources", organized by UNU-GTP and LaGeo, in Ahuachapan and Santa Tecla, El Salvador, 17-30 October, 2009.

Rosyidi S.A., Taha M.R., Lesmana S.B., Wintolo J. and Adi A.D., (2008), Some lessons from Yogyakarta earthquake of May 27, 2006: Proceeding of 6th International Conference on Case Histories in Geotechnical Engineering, Arlington Virginia, 11 – 16 August 2008.

Sharma P. V., (2002), Environmental and Engineering Geophysics 1st. Edn., Cambridge University Press, pp. 226, 227.

Sheriff R.E., (1994), Encyclopaedic dictionary of exploration geophysics 3rd. Edn., SEG – Society of Exploration Geophysics.

Simiyu S. M. and Keller G. R., (2001), An integrated geophysical analysis of the upper crust of the Southern Kenya rift: *Geophysical Journal International*, **147**, 543–561

Simiyu S. M., (2009), Application of micro-seismic method to geothermal exploration from the Kenya Rift: U. N. Short Course for Exploration for Geothermal Resources.

Simiyu S.M., Omenda P.A., Anthony E.Y. and Keller G.R., (1995), Geophysical and geological evidence for the occurrence of shallow magmatic intrusions in the Naivasha sub-basin of the Kenya Rift: EOS Transactions of the AGU, **76**, 257–258.

Swain C.J., Maguire P.K.H. and Khan M.A., (1994), Geophysical experiments and models of the Kenya Rift before 1989: *Journal of Tectonophysics*, **236**, 23-32.

Telford W.M., Geldart L.P. and Sheriff R.E., (1990), *Applied Geophysics*, 2nd edn. Cambridge University Press, Cambridge.

Vincent B.J, (2000), Mapping the Springville system using gravity surveys, supported by magnetic data: Master's thesis, Brigham Young University.

Wamalwa A.M, Kevin L. M., Laura F. S., (2013), Geophysical characterization of the Menengai volcano, Central Kenya Rift from the analysis of magnetotelluric and gravity data: *Journal of Geophysics*, **78**, 187–199.

Young P., Maguire P., Laffoley A., and Evans J., (1991), Implications of the distribution of seismic activity near Lake Bogoria in the Kenya rift. *Geophysics Journal International*, **105**, 665-674.

APPENDICES

These appendices include geophysical data for each of the three methods. Station locations are given in WGS 84, zone 37 S, UTM Coordinates. Elevation data are in metres. Gravity data is in mGal, magnetic data in nT and resistivity data in Ωm.

A1: VES DATA

Mn/2 (m)	AB/2 (m)	VES 1. (Ωm)	VES 2. (Ωm)	VES 3. (Ωm)	VES 4. (Ωm)
0.50	1.60	140.18	129.69	210.81	154.91
0.50	2.00	116.33	117.01	200.56	177.06
0.50	2.50	105.53	105.95	194.29	214.49
0.50	3.20	95.99	101.85	179.96	251.78
0.50	4.00	93.00	89.57	176.37	286.91
0.50	5.00	85.98	89.29	177.81	313.61
0.50	6.30	77.36	85.11	172.61	347.37
0.50	8.00	66.25	77.67	166.61	367.18
0.50	10.00	58.16	70.62	184.57	386.65
0.50	13.00	54.00	67.25	151.45	385.67
0.50	16.00	55.54	70.89	131.14	361.03
0.50	20.00	62.66	80.70	105.73	315.93
10.00	25.00	72.60	88.51	96.61	241.65
10.00	32.00	84.07	105.40	95.20	189.77
10.00	40.00	90.19	110.46	101.82	142.22
10.00	50.00	101.46	113.40	112.20	129.11
10.00	63.00	108.09	110.25	128.78	124.96
25.00	80.00	128.84	107.52	149.61	161.24
25.00	100.00	122.55	114.48	199.55	144.87
25.00	130.00	121.09	113.34	167.26	160.05
25.00	160.00	126.63	119.48	156.82	175.29
25.00	200.00	108.37	117.21	185.65	164.80
25.00	250.00	79.27	100.72	188.92	150.55

Mn/2 (m)	AB/2 (m)	VES 5. (Ωm)	VES 6. (Ωm)	VES 7. (Ωm)	VES 8. (Ωm)
0.50	1.60	304.28	213.97	212.35	156.22
0.50	2.00	352.15	196.16	187.93	124.25
0.50	2.50	415.57	183.08	165.82	132.15
0.50	3.20	480.23	156.59	130.19	127.12
0.50	4.00	399.25	147.90	110.38	145.08
0.50	5.00	333.70	143.61	93.87	160.88
0.50	6.30	249.65	149.14	75.97	171.74
0.50	8.00	172.85	156.49	62.89	175.61
0.50	10.00	140.08	163.02	52.68	186.12
0.50	13.00	92.88	165.76	53.92	178.77
0.50	16.00	78.21	168.86	61.99	155.29
0.50	20.00	110.88	175.43	75.16	131.96
10.00	25.00	106.96	180.57	77.78	113.06
10.00	32.00	89.19	200.04	93.82	121.77
10.00	40.00	100.67	211.63	105.75	98.00
10.00	50.00	117.25	227.84	111.60	101.46
10.00	63.00	124.61	244.07	106.89	103.86
25.00	80.00	160.65	291.35	122.43	126.79
25.00	100.00	183.50	299.56	139.86	135.36
25.00	130.00	181.96	318.56	159.33	133.65
25.00	160.00	160.98	282.74	160.62	129.80
25.00	200.00	164.70	279.41	161.80	124.70
25.00	250.00	131.35	306.92	141.08	102.41

A2: HEP DATA

a) HEP-1.

St. No.	Eastings (m)	Northings (m)	Resistivity (ρm)
1	169981	9969016	106.06
2	169979	9969010	95.73
3	169989	9969006	99.78

4	170017	9969012	104.52
5	170017	9969012	48.86
6	170023	9969012	46.18
7	170038	9969010	41.37
8	170040	9969012	40.93
9	170047	9969010	41.15
10	170065	9969012	45.52
11	170075	9969012	46.84
12	170083	9969008	46.88
13	170087	9969012	52.3
14	170102	9969022	46.09
15	170111	9969006	43.9
16	170131	9969016	44.59
17	170139	9969038	43.21
18	170147	9969004	43.92
19	170157	9969014	44.17
20	170171	9969012	42.17
21	170173	9969006	39.59
22	170180	9969012	92.03
23	170198	9969010	93.9
24	170208	9969008	100.99
25	170217	9969008	109.87
26	170226	9969004	103.61
27	170245	9968992	103.61
28	170245	9969002	62.36
29	170257	9969000	54.94
30	170271	9968996	61
31	170278	9968998	82.76
32	170286	9968996	126.83
33	170298	9968998	143.49
34	170306	9968992	102.41
35	170315	9968994	51.11

36	170325	9968992	62.22
37	170337	9968992	83.24
38	170349	9968988	73.78
39	170359	9968990	69.49
40	170371	9968988	88.18
41	170379	9968988	87.84
42	170386	9968988	88.87
43	170397	9968988	88.89
44	170416	9968988	72.86
45	170423	9968986	82.31
46	170430	9968930	84.48
47	170439	9968984	78.81
48	170447	9968990	87.15
49	170461	9968990	80.99
50	170471	9968992	89.84
51	170474	9968992	97.56
52	170487	9968990	84.61
53	170497	9968992	90.95
54	170509	9968990	100.39
55	170520	9968992	110.27
56	170530	9968992	99.84
57	170537	9968988	93.36
58	170546	9968988	91.86
59	170549	9968988	93.5
60	170569	9968990	62.23
61	170575	9968988	94.15
62	170593	9968992	103.61
63	170600	9968992	107.84
64	170619	9968990	100.33
65	170622	9968990	90.52
66	170628	9968992	80.52
67	170644	9968992	156.3

68	170652	9968994	245.59
69	170661	9968994	197.71

b) HEP-2.

St. No.	Eastings (m)	Northings (m)	Resistivity (ρm)
1	169058	9969632	551.2
2	169058	9969638	550.12
3	169078	9969642	551.2
4	169084	9969646	546.3
5	169093	9969650	548.11
6	169103	9969656	539.23
7	169111	9969654	526.25
8	169122	9969658	519.96
9	169137	9969662	475.21
10	169145	9969666	411.2
11	169157	9969672	410.21
12	169165	9969674	401.2
13	169174	9969678	395.63
14	169184	9969680	382.2
15	169193	9969684	379.23
16	169203	9969688	369.85
17	169215	9969692	350.54
18	169227	9969698	216.7
19	169240	9969702	214.6
20	169253	9969704	214.21
21	169265	9969708	190.36
22	169277	9969710	194.89
23	169288	9969714	198.92
24	169301	9969714	195.24
25	169314	9969714	199.87
26	169326	9969718	197.63

27	169339	9969718	199.37
28	169352	9969718	201.44
29	169362	9969718	358.69
30	169376	9969720	371.22
31	169389	9969718	381.78
32	169401	9969716	385.26
33	169415	9969716	396.22
34	169425	9969714	409.22
35	169439	9969712	439.47
36	169452	9969708	460.59
37	169467	9969706	478.56
38	169481	9969702	482.45
39	169492	9969698	489.2
40	169505	9969696	501.2
41	169513	9969694	505.98
42	169523	9969688	516.9
43	169532	9969684	521.56
44	169542	9969680	519.97
45	169552	9969674	517.21
46	169562	9969670	529.26
47	169564	9969668	530.01
48	169585	9969660	528.22
49	169598	9969652	532.21
50	169609	9969644	536.59
51	169620	9969638	542.22
52	169630	9969632	540.26
53	169637	9969626	541.58
54	169649	9969620	546.56
55	169660	9969614	543.22
56	169669	9969608	549.29
57	169680	9969604	551.72
58	169689	9969600	547.23

59	169697	9969594	542.57
60	169708	9969588	539.36
61	169717	9969582	522.59
62	169729	9969574	516.24
63	169737	9969570	512.32
64	169747	9969566	511.59
65	169756	9969562	509.89
66	169767	9969558	510.55
67	169775	9969554	502.57
68	169786	9969550	500.47
69	169797	9969546	501.69
70	169808	9969544	500.89
71	169819	9969542	506.83
72	169832	9969540	499.26
73	169842	9969540	512.22
74	169852	9969540	519.24
75	169862	9969540	517.84
76	169872	9969540	519.87
77	169882	9969542	520.42
78	169892	9969544	521.12
79	169902	9969546	519.92
80	169912	9969546	521.85
81	169923	9969550	516.89
82	169933	9969554	509.24
83	169942	9969556	501.87
84	169951	9969560	499.54
85	169961	9969564	506.56
86	169971	9969566	509.23
87	169980	9969572	502.25
88	169985	9969590	500.12
89	169994	9969590	506.16
90	170004	9969594	509.58

91	170015	9969596	502.45
92	170024	9969600	500.98
93	170035	9969608	497.22
94	170048	9969612	489.26
95	170055	9969618	487.26
96	170061	9969620	486.56
97	170069	9969624	481.31
98	170077	9969628	485.64
99	170089	9969634	489.23
100	170101	9969642	478.29
101	170111	9969648	471.22
102	170120	9969652	468.63
103	170130	9969658	479.65
104	170141	9969660	475.23
105	170154	9969668	489.29
106	170168	9969674	489.98
107	170180	9969680	492.58
108	170189	9969686	496.58
109	170203	9969696	492.22
110	170210	9969698	497.22
111	170218	9969700	490.25
112	170227	9969704	498.55
113	170239	9969710	500.23
114	170247	9969716	507.99
115	170258	9969722	519.15
116	170269	9969728	523.51
117	170277	9969734	529.59
118	170288	9969740	530.75
119	170299	9969744	536.25
120	170308	9969750	539.59
121	170320	9969756	541.58
122	170331	9969760	554.98

123	170341	9969764	552.69
124	170351	9969766	543.25
125	170360	9969768	549.6
126	170371	9969770	551.58
127	170382	9969772	556.7
128	170390	9969764	559.62
129	170401	9969774	542.6
130	170412	9969776	549.26
131	170422	9969776	541.51
132	170433	9969776	539.25
133	170442	9969774	530.22
134	170453	9969774	529.15
135	170466	9969774	428.01
136	170477	9969770	421.25
137	170485	9969768	422.65
138	170495	9969764	419.25
139	170503	9969760	422.69
140	170514	9969756	416.2
141	170525	9969752	414.36
142	170535	9969748	417.26
143	170545	9969742	412.29
144	170555	9969736	419.02
145	170564	9969730	411.21
146	170573	9969722	408.27
147	170581	9969716	406.06
148	170589	9969710	407.82
149	170594	9969702	402.99
150	170603	9969694	400.22
151	170611	9969688	406.2
152	170618	9969680	409.55
153	170625	9969668	411.35
154	170632	9969662	406.22

155	170638	9969654	378.69
156	170642	9969644	356.63
157	170649	9969636	346.96
158	170659	9969628	348.59
159	170667	9969620	329.6
160	170674	9969612	344.6
161	170681	9969604	349.24
162	170688	9969596	340.23
163	170695	9969588	337.98
164	170701	9969580	342.44
165	170709	9969570	347.62
166	170715	9969562	375.92
167	170721	9969554	398.26
168	170728	9969546	442.22
169	170734	9969538	456.6
170	170741	9969528	451.22
171	170749	9969522	478.22
172	170756	9969512	469.28
173	170764	9969504	456.25
174	170770	9969498	444.96
175	170778	9969490	439.59
176	170787	9969482	432.69
177	170796	9969476	438.57
178	170806	9969470	441.29
179	170815	9969464	436.51
180	170825	9969458	392.63
181	170834	9969454	389.5
182	170844	9969450	409.45
183	170854	9969446	406.89
184	170866	9969442	401.35
185	170871	9969442	397.05
186	170877	9969440	391.56

187	170885	9969436	399.59
188	170898	9969436	390.28
189	170907	9969434	392.59
190	170922	9969432	398.26

A3: GRAVITY DATA

S. No.	UTM Coordinates		Elevation (m)	Raw Gravity (G.U)	Corrected Gravity (G.U)
	Eastings (m)	Northings (m)			
1	169403	9969040	1894	11291.6	15016.63115
2	169491	9969054	1898	11311.7	15044.58502
3	169573	9969052	1895	11298.7	15025.64408
4	169655	9969044	1884	11310.7	15016.01309
5	169706	9969110	1881	11296.5	14995.95695
6	169811	9969090	1893	11300	15023.01523
7	169898	9969090	1895	11299.8	15026.80311
8	169964	9969088	1892	11304.6	15025.67809
9	170019	9969092	1896	11306.9	15035.88369
10	170088	9969002	1884	11313.8	15019.14343
11	170148	9968990	1881	11320.9	15020.30973
12	170180	9968988	1882	11324.8	15026.24448
13	170224	9968984	1881	11328.4	15027.83927
14	170294	9968962	1877	11340.7	15032.31658
15	170334	9968956	1878	11332.9	15026.47178
16	170389	9968950	1874	11341.5	15027.18843
17	170441	9968950	1874	11345.7	15031.40492
18	170484	9968590	1875	11351	15038.60227
19	170539	9968948	1865	11352	15019.95663
20	170583	9968952	1866	11356.6	15026.49762
21	170625	9968950	1866	11357	15026.96364
22	170683	9968950	1875	11342.2	15029.86236

23	170719	9968950	1874	11342.7	15028.35566
24	170728	9969050	1876	11337.1	15026.72679
25	170684	9969052	1879	11334.2	15029.73313
26	170642	9969066	1869	11352.2	15028.03332
27	170594	9969068	1873	11347.3	15031.03362
28	170552	9969070	1874	11343.7	15029.4041
29	170504	9969076	1876	11341.1	15030.70631
30	170456	9969076	1867	11337.4	15009.30576
31	170408	9969078	1872	11333.7	15015.39338
32	170352	9969084	1881	11328.1	15027.52105
33	170316	9969086	1882	11323.6	15025.03842
34	170287	9969092	1880	11332.1	15029.54653
35	170248	9969092	1886	11320.3	15029.61694
36	170211	9969094	1885	11315.8	15023.1409
37	170181	9969098	1886	11314.8	15024.09732
38	170140	9969100	1889	11313.3	15028.46385
39	170095	9969106	1893	11309.5	15032.48386
40	170050	9969110	1897	11307	15037.87175
41	170004	9969128	1894	11305.3	15030.25772
42	169964	9969154	1897	11301.7	15032.56848
43	169913	9969188	1898	11300.7	15033.53171
44	169883	9969192	1897	11300.1	15030.97155
45	169833	9969192	1897	11301.3	15032.24775
46	169773	9969194	1897	11297.9	15028.76678
47	169715	9969180	1897	11294.8	15025.74664
48	169695	9969244	1892	11295	15016.02544
49	169665	9969314	1895	11288.5	15015.44065
50	169620	9969354	1900	11279.5	15016.30546
51	169595	9969310	1899	11293.7	15028.51307
52	169554	9969292	1906	11287.4	15036.0371
53	169505	9969272	1906	11283.6	15032.24491
54	169459	9969244	1902	11285.5	15026.26821

55	169420	9969214	1902	11280.9	15021.66024
56	169397	9969210	1904	11278.6	15023.31659
57	169413	9969250	1906	11275.6	15024.17238
58	169453	9969280	1900	11283.2	15020.05511
59	169552	9969358	1905	11277.8	15024.45785
60	169822	9969408	1906	11279.4	15028.01701
61	169855	9969294	1907	11298	15048.60747
62	169959	9969282	1900	11304.7	15041.54507
63	169084	9969268	1893	11308.9	15031.94528
64	169168	9969276	1891	11309.1	15028.22215
65	169262	9969272	1872	11323.7	15005.48354
66	169322	9969278	1886	11315.2	15024.4916
67	170287	9969162	1879	11327	15022.46801
68	170592	9969142	1872	11344.3	15026.06568
69	170709	9969274	1884	11319.7	15025.05806
70	170730	9969382	1890	11312.8	15029.98135
71	170642	9969494	1893	11308	15031.04673
72	170665	9969598	1911	11279.7	15038.23027
73	170714	9969624	1912	11275.8	15036.19011
74	170671	9969782	1929	11255	15048.83824
75	170542	9969844	1925	11267.7	15053.68854
76	170434	9969884	1920	11279.8	15055.97141
77	170315	9969756	1905	11277.6	15024.26986
78	170144	9969662	1921	11270	15048.10689
79	170245	9969598	1900	11293.2	15029.98015
80	170228	9969513	1894	11305.5	15030.46482
81	170181	9969504	1894	11301.6	15026.63185
82	170047	9969480	1917	11292.2	15062.4237
83	169948	9969582	1935	11262.9	15068.53037
84	169808	9969542	1932	11257.6	15057.36058
85	169626	9969646	1919	11243.2	15017.35422
86	169468	9969706	1930	11241	15036.8275

87	169347	9969626	1913	11244.9	15007.31763
88	169227	9969692	1917	11239.5	15009.73219
89	169235	9969910	1937	11215.5	15025.05057
90	169412	9970079	1940	11206.6	15022.1066
91	169752	9969964	1940	11216.6	15032.03768
92	169930	9969974	1925	11225.3	15011.23646
93	169995	9970115	1940	11218.2	15033.66757
94	169956	9970334	1950	11204	15039.14882
95	170092	9970365	1951	11183.9	15021.0582
96	170192	9970186	1954	11216.2	15059.26944
97	170328	9970026	1941	11251.5	15068.9691
98	170327	9970178	1943	11217.2	15038.61601
99	170418	9970220	1947	11206.7	15035.96825
100	170563	9970316	1985	11142.5	15046.54193
101	170684	9970264	1990	11133	15046.81365
102	170843	9970254	1998	11125.2	15054.73481
103	170835	9970094	1966	11150.4	15017.04954
104	170646	9970000	1937	11230.8	15040.38936
105	170893	9969732	1925	11239.9	15025.87875
106	171055	9969666	1920	11259.8	15035.95697
107	170918	9969466	1909	11289.8	15044.36612
108	170972	9969376	1889	11325.4	15040.54971
109	170946	9969168	1861	11346.9	15006.97281
110	170103	9969950	1924	11310.7	15094.75232
111	169863	9969822	1926	11310.9	15098.85729
112	169666	9969810	1922	11311.1	15091.17377
113	169438	9969886	1927	11311.2	15101.12311
114	169305	9969800	1931	11311.4	15109.17749
115	169022	9969838	1934	11311.7	15115.32396
116	168912	9969636	1933	11311.8	15113.50977
117	168583	9969566	1931	11312	15109.78368
118	168628	9969398	1929	11312.3	15106.09747

119	168581	9969274	1926	11312.8	15100.76061
120	168961	9969114	1934	11313.2	15116.90525
121	169127	9968996	1902	11313.5	15054.18802
122	169395	9968862	1903	11313.7	15056.40602
123	169620	9968832	1902	11313.9	15054.64072
124	169703	9968776	1889	11314.5	15029.65339
125	169917	9968708	1897	11314.6	15045.52783
126	170056	9968604	1877	11314.8	15006.34165
127	170119	9968588	1872	11314.9	14996.60369
128	170266	9968516	1868	11315	14988.8504
129	170414	9968470	1867	11315.2	14987.05716
130	170378	9968668	1870	11315.4	14993.20063
131	170497	9968652	1860	11315.5	14973.60904
132	170680	9968648	1859	11315.8	14971.99529
133	170614	9968804	1866	11315.9	14985.8671
134	170470	9968884	1868	11316.1	14989.93017
135	170345	9968880	1870	11316.2	14994.03713
136	170179	9968904	1884	11316.4	15021.75987
137	170085	9968808	1884	11316.6	15021.89247
138	170061	9968894	1877	11316.7	15008.29381
139	170005	9968948	1883	11317	15020.34249

A4: MAGNETIC DATA

S. No.	UTM Coordinates		Raw Field Reading (nT)	Corrected Field (nT)
	Eastings (m)	Northings (m)		
1	170174	9969156	33550.8	33547.3
2	170222	9969160	33533.2	33529.7
3	170254	9969160	33516.4	33513
4	170288	9969158	33504.2	33500.8
5	170318	9969150	33501.6	33498.2
6	170355	9969150	33499.2	33496

7	170397	9969148	33483.2	33480.4
8	170442	9969146	33480.4	33477.6
9	170496	9969146	33490.4	33487.4
10	170513	9969144	33489.2	33485.7
11	170536	9969140	33499.4	33495.8
12	170566	9969142	33505.4	33500.9
13	170597	9969138	33493	33488
14	170626	9969138	33472.8	33467.8
15	170650	9969132	33473.4	33468.4
16	170673	9969132	33469	33464.4
17	170658	9969072	33411.4	33412.9
18	170641	9969078	33429.6	33431.6
19	170625	9969074	33419.6	33422
20	170601	9969078	33434.4	33436.8
21	170578	9969076	33449.2	33451.6
22	170553	9969080	33458.6	33461.1
23	170523	9969082	33472.6	33475.3
24	170494	9969082	33482.2	33485
25	170470	9969078	33487.8	33490.7
26	170416	9969090	33484.4	33488.3
27	170382	9969082	33477.2	33481.1
28	170337	9969090	33482.2	33486
29	170311	9969088	33491.8	33494.1
30	170290	9969082	33491.8	33494.2
31	170286	9969084	33490	33492.3
32	170281	9969076	33488.2	33490
33	170266	9969076	33486.8	33488.6
34	170250	9969074	33485.2	33486.8
35	170226	9969072	33487.8	33489.4
36	170204	9969080	33489.8	33489.8
37	170181	9969076	33488.8	33488.6
38	170153	9969080	33486.4	33486.4

39	170132	9969082	33486.4	33486.8
40	170122	9969080	33488.8	33489.5
41	170095	9969084	33497.2	33498
42	170074	9969084	33505.4	33506.3
43	170051	9969086	33514.2	33516.7
44	170033	9969088	33520.6	33524.4
45	170013	9969092	33521	33525.2
46	169984	9969096	33530	33534.4
47	169953	9969104	33539.2	33544
48	169955	9969040	33507.2	33510
49	169974	9969040	33483.2	33484.8
50	170003	9969034	33481.8	33483.2
51	170018	9969032	33480.2	33481.6
52	170040	9969036	33479.2	33480.6
53	170073	9969034	33475	33477
54	170101	9969036	33477	33479.4
55	170139	9969030	33480.2	33482.7
56	170181	9969032	33479.6	33482.8
57	170218	9969022	33487.8	33491.9
58	170268	9969038	33492.4	33496.6
59	170297	9969038	33491	33495.3
60	170324	9969030	33499	33503.6
61	170355	9969028	33502	33506.6
62	170390	9969030	33504.8	33509.6
63	170411	9969024	33502	33506.9
64	170440	9969022	33491.2	33496.3
65	170478	9969020	33484.2	33489.4
66	170501	9969020	33483.6	33488.8
67	170533	9969020	33480.6	33485.9
68	170569	9969018	33474	33479.3
69	170593	9969020	33456.2	33461.6
70	170622	9969018	33430.4	33435.9

71	170642	9969016	33401.2	33406.8
72	170671	9969012	33419	33424.6
73	170701	9968992	33434.6	33440.2
74	170680	9968994	33421.2	33427.2
75	170663	9968994	33418.2	33424.4
76	170705	9968960	33458.2	33466.8
77	170678	9968960	33456.6	33465.2
78	170652	9968958	33449.8	33458.4
79	170638	9968956	33448	33456.6
80	170607	9968956	33457	33465.6
81	170575	9968952	33470	33478.6
82	170528	9968952	33472	33480.6
83	170500	9968954	33469.8	33478.4
84	170461	9968954	33476.2	33484.8
85	170429	9968956	33481.2	33490.8
86	170396	9968960	33481.4	33491.2
87	170357	9968960	33494	33503.9
88	170328	9968960	33498.6	33508.8
89	170306	9968958	33499.8	33510.3
90	170289	9968958	33505.4	33516.3
91	170261	9968952	33516	33527
92	170233	9968952	33526.2	33537.2
93	170199	9968948	33512	33523.1
94	170183	9968948	33502.8	33514
95	170153	9968948	33491.4	33502.7
96	170123	9968942	33490.2	33501.7
97	170090	9968942	33486.8	33498.5
98	170059	9968944	33488.8	33500.6
99	170034	9968944	33487.6	33499.6
100	170001	9968942	33487.2	33499.2
101	169972	9968952	33488	33500
102	169931	9968932	33481.2	33493.2

103	169959	9968910	33472.8	33485.5
104	169962	9968894	33443.8	33459
105	170017	9968856	33412.4	33428.4
106	170052	9968858	33427	33443.2
107	170108	9968884	33458	33473.4
108	170132	9969180	33492.6	33529.4
109	170104	9969196	33465.6	33502.8
110	170112	9969196	33467.4	33502.2
111	170075	9969174	33480.6	33516.2
112	170039	9969170	33485.8	33521.8
113	170010	9969162	33499.2	33535.5
114	169978	9969164	33503.8	33540.5
115	169962	9969164	33507.8	33544.7
116	169935	9969232	33431.6	33468.2
117	169981	9969244	33449.4	33486
118	170035	9969242	33469.2	33505.8
119	170080	9969242	33485.6	33522.2
120	170080	9969272	33497.8	33534.8
121	170074	9969272	33509	33546.4
122	170048	9969272	33525.4	33562.8
123	170009	9969274	33526.2	33563.6
124	169970	9969276	33537.8	33575.2
125	169934	9969280	33528.2	33565.6
126	169894	9969284	33545.4	33583.2
127	169779	9969314	33502.8	33541.5
128	169824	9969220	33479.8	33519.8
129	169820	9968950	33468.8	33512
130	170192	9969200	33487.8	33531.8
131	170231	9969214	33483.2	33527.6
132	170252	9969216	33473.8	33518.2
133	170282	9969218	33451.8	33496.2
134	170315	9969216	33454	33498.5

135	170301	9969276	33441.8	33486.4
136	170114	9968870	33474.2	33462.2
137	170102	9968832	33432.2	33418.2
138	170068	9968812	33414.8	33399.8
139	170026	9968818	33400.8	33384.8
140	169961	9968828	33393.8	33376.8
141	169961	9968872	33415	33396.8
142	169923	9968874	33438.8	33420
143	169798	9968898	33464.2	33444.5
144	169768	9968930	33470.6	33450.4
145	169766	9968978	33491.6	33470.6
146	169724	9969005	33504.8	33481.3
147	169703	9969124	33562.8	33535.8
148	169703	9969158	33566.4	33538
149	169689	9969232	33557.4	33528.4
150	169679	9969302	33471	33440
151	169609	9969374	33496.8	33463.8
152	169572	9969376	33470.4	33436.8
153	169586	9969320	33494.2	33459.7
154	169608	9969286	33550.8	33514.6
155	169621	9969208	33515.6	33473
156	169636	9969162	33580.8	33537.4
157	169681	9968990	33494.4	33451.4
158	168927	9969162	33533.2	33485.2
159	168926	9969138	33549.2	33500.8
160	168944	9969092	33550.6	33501
161	169108	9969026	33558.2	33509.2
162	169316	9969810	33462.8	33413.3
163	170153	9968110	33475.8	33428.2
164	170154	9968196	33462.6	33417
165	170194	9968204	33460.6	33415.6
166	170305	9968218	33520.4	33477.4

167	170344	9968198	33485.2	33442.3
168	170375	9968190	33483.8	33442.6
169	170397	9968192	33510.6	33469.4
170	170417	9968216	33492.8	33451.6
171	170459	9968226	33455.2	33414
172	170499	9968224	33504.8	33462.8
173	170573	9968388	33522.2	33482.2
174	170546	9968408	33503.2	33464
175	170477	9968456	33506.6	33468.6
176	170062	9968544	33469.2	33434.8
177	170014	9968540	33462.8	33429.3
178	169966	9968530	33468.2	33435.2
179	169949	9968558	33465.4	33434.4
180	170445	9968634	33438.6	33414.3
181	170450	9968694	33427.8	33404.2
182	170442	9968750	33429.4	33406.4
183	170495	9968740	33452.8	33430.4
184	170540	9968812	33441.2	33420.7
185	170593	9968802	33446	33427.1
186	170134	9969382	33469.8	33484.6
187	170080	9969356	33490.4	33505.4
188	169969	9969364	33428.2	33444.8
189	169050	9969394	33476.6	33493.8
190	169072	9969404	33444	33462
191	169097	9969408	33507.8	33526.2
192	170040	9969416	33541.8	33560
193	170070	9969418	33467.8	33485.7
194	170129	9969420	33513	33531.1
195	170156	9969412	33529.4	33547.9
196	170235	9969428	33515.4	33534.4
197	170249	9969426	33510.4	33529.4
198	170245	9969472	33463.2	33482.4

199	170234	9969520	33500.8	33520
200	170155	9969494	33456.8	33476.1
201	170116	9969490	33463.8	33482.6
202	170098	9969520	33500.8	33519.9
203	170037	9969496	33443.6	33462.4
204	169989	9969490	33497	33516
205	169952	9969474	33512.2	33531.5
206	169903	9969478	33523.6	33543.2
207	169881	9969512	33532.6	33552.4
208	169822	9969480	33547	33567.1
209	169791	9969536	33534.4	33554.7
210	169926	9969528	33558	33578.6
211	170019	9969522	33529	33551.4
212	170148	9969582	33526.6	33550.8
213	170199	9969628	33510.6	33535.6
214	170236	9969598	33501.4	33527.9
215	170178	9969596	33525	33552
216	170522	9968924	33438.8	33466.2
217	170579	9968922	33436.2	33463.6
218	170634	9968920	33413.8	33440.8
219	170686	9968916	33420	33446.8
220	170688	9968878	33428	33454.6
221	170656	9968874	33397.2	33423.7
222	170625	9968870	33408.2	33434.4
223	170590	9968866	33409.6	33435.7
224	170558	9968866	33414	33440.1
225	170523	9968870	33418.4	33444.4
226	170482	9968804	33397	33422.8
227	170531	9968790	33403.8	33428.8
228	170578	9968780	33401.4	33427.6
229	170628	9968778	33408	33434.6
230	170637	9968814	33403	33428

231	170634	9968714	33401.6	33427.3
232	170616	9968670	33400	33425.6
233	170614	9968626	33403.6	33429.2
234	170628	9968586	33411.6	33436.9
235	170669	9968572	33410.6	33434.6
236	170705	9968558	33420	33443.5
237	170580	9968582	33397	33419.8
238	170535	9968626	33426.6	33448.8
239	170465	9968640	33390.6	33412.1
240	170183	9969158	33546.2	33541.8
241	170251	9969156	33517	33513.3
242	170288	9969158	33505.4	33501.8
243	170309	9969154	33502.8	33499.4
244	170336	9969152	33495.8	33492.6
245	170389	9969150	33485.6	33481.6
246	170444	9969148	33477.6	33418.5
247	170506	9969142	33493	33488.5
248	170553	9969142	33505.4	33500.5
249	170578	9969138	33493.4	33488.4
250	170642	9969136	33475.4	33470.2
251	170673	9969134	33467.2	33461.8
252	170704	9969022	33465	33458.8
253	170679	9968946	33465.2	33458.4
254	170700	9968964	33470	33463.3
255	170962	9969326	33507.6	33499.5
256	170975	9969376	33498	33489.6
257	170935	9969412	33484	33474.9
258	170876	9969414	33582	33572.5
259	170826	9969442	33566	33556.4
260	170783	9969456	33601.4	33591.8
261	170872	9969546	33508	33499.9
262	170871	9969582	33474.6	33468.4

263	170752	9969638	33499.4	33494.2
264	170731	9969644	33542	33536.9
265	170732	9969612	33448.4	33443.7
266	170712	9969631	33544.8	33540.7
267	170746	9969690	33635.4	33631.4
268	170718	9969684	33583	33579
269	170672	9969688	33534.8	33531
270	170640	9969720	33566.2	33562.3
271	170612	9969756	33536.6	33532.2
272	170590	9969780	33544.2	33539.3
273	170519	9969788	33558	33553
274	170468	9969868	33518	33512.4
275	170421	9969876	33492	33486.3
276	170405	9969830	33533	33527.5
277	170376	9969832	33537.6	33532.5
278	170365	9969890	33507.6	33503.3
279	170374	9969984	33614.4	33610.8
280	170371	9970032	33623.4	33622
281	170396	9970046	33628	33626.6
282	170430	9970232	33560.8	33560
283	170878	9970168	33576	33575.6
284	170824	9970160	33570	33569.4
285	170846	9970108	33566.2	33566.5
286	170910	9970114	33561.6	33561.6
287	170914	9970056	33559.8	33559.8
288	170876	9970052	33553	33553
289	170816	9970042	33599.4	33602.5
290	170794	9970026	33591.8	33594.7
291	170766	9969882	33549.2	33552.4
292	170901	9969698	33537	33541.2
293	170984	9969632	33533.2	33537.3
294	171011	9969570	33452.6	33457.1

295	171005	9969538	33411.4	33416.5
296	170960	9969554	33460.2	33465.4
297	170939	9969514	33455.2	33460.7
298	170917	9969468	33465.8	33471.6
299	170181	9969714	33604	33613.5
300	170168	9969636	33539.4	33550.4
301	170474	9968442	33448.8	33484.2
302	170499	9968264	33422.2	33459.8
303	170439	9968264	33428	33466.4
304	170413	9968220	33436.8	33475.8
305	170396	9968212	33437.8	33477
306	170366	9968214	33426.8	33466.3
307	170325	9968206	33403.8	33443.8
308	170301	9968220	33429	33469.4
309	170326	9968216	33429.2	33469.4
310	170230	9968214	33478.4	33520
311	170189	9968210	33421.2	33465.4
312	170172	9968216	33396.8	33441.2
313	170194	9968314	33407.8	33452.9
314	170153	9968350	33420.8	33465
315	170061	9968376	33403	33449.1
316	170026	9968390	33394.4	33440.6
317	169983	9968400	33396.6	33442.9
318	169978	9968480	33404	33451.2
319	170022	9968502	33392	33439.6
320	170068	9968518	33392.8	33440.8
321	169478	9969272	33471.2	33470
322	169459	9969256	33578.2	33576.4
323	169410	9969204	33565.8	33563.8
324	169365	9969232	33622.8	33620.5
325	169328	9969474	33423.2	33419.4
326	169348	9969472	33601.2	33598

327	169367	9969482	33440.6	33437.4
328	169365	9969506	33399	33393.4
329	169370	9969500	33518.4	33513
330	169488	9969572	33635	33626.6
331	169524	9969566	33635	33626
332	169561	9969482	33532.8	33523
333	169553	9969446	33463.8	33453.7
334	169556	9969414	33422.8	33412.2
335	169573	9969374	33459	33448.4
336	169587	9969318	33481.6	33470.9
337	169597	9969300	33574	33563.2
338	169614	9969292	33530.4	33519.6
339	169633	9969286	33490.2	33479.9
340	169610	9969230	33533	33524
341	169178	9969606	33556	33547.1
342	169129	9969616	33559.2	33550.4
343	169081	9969678	33554.2	33545.1
344	169040	9969654	33493	33483.7
345	168969	9969634	33584	33575
346	168917	9969602	33644.6	33635.6
347	168809	9969582	33615.4	33606.4
348	168911	9969726	33568.4	33559.4
349	168987	9969740	33525.4	33516.6
350	168995	9969830	33549.8	33542
351	169072	9969774	33530.4	33520.6
352	169022	9969950	33588	33576
353	169178	9970178	33657.6	33648.4
354	169218	9970278	33663.6	33654.8
355	169490	9970104	33592	33581.8
356	169526	9970152	33594.6	33583.1
357	169477	9970230	33601	33588.9
358	169952	9970000	33609.6	33596.5

359	169940	9969804	33599.6	33584.6
360	169958	9969726	33558.6	33544.7
361	169836	9969634	33621.6	33609.2
362	169628	9969670	33660.8	33648
363	169820	9969508	33622.8	33608.9
364	169846	9969526	33637.2	33623.2
365	170137	9969160	33545.2	33531.2